NOAA Technical Memorandum ERL PMEL-33

EDDIES DETACHED FROM A JET CROSSING OVER A SUBMARINE RIDGE USING A SIMPLE NUMERICAL MODEL

Motoyoshi Ikeda

Pacific Marine Environmental Laboratory
Seattle, Washington
December 1981

UNITED STATES
DEPARTMENT OF COMMERCE
Malcolm Baldrige,
Secretary

NATIONAL OCEANIC AND
ATMOSPHERIC ADMINISTRATION
John V. Byrne,
Administrator

Environmental Research
Laboratories
George H. Ludwig
Director

NOTICE

Mention of a commercial company or product does not constitute an endorsement by NOAA Environmental Research Laboratories. Use for publicity or advertising purposes of information from this publication concerning proprietary products or the tests of such products is not authorized.

CONTENTS

EDDIES DETACHED FROM A JET CROSSING OVER A SUBMARINE RIDGE USING A SIMPLE NUMERICAL MODEL[1]

Motoyoshi Ikeda

ABSTRACT. An eastward-flowing jet crossing over a submarine ridge is studied using a two-layer quasi-geostrophic model. The jet initially has small-amplitude meanders of one wavelength to the west of the ridge, and the lower layer is quiescent only at t = 0. The meanders grow propagating eastward, and the lower layer begins to move and feel bottom topography. Then, the ridge influences meanders and eddies that are detached from large-amplitude meanders. Detached, cyclonic eddies are strengthened south of the jet on the western slope of the ridge, as are anticyclonic eddies north of the jet on the eastern slope, because of vorticity generated by the topographic effects on the westward flows associated with two recirculating gyres which form on the north and south of the jet. Consistent with topographic Rossby wave theory, some of these eddies approach and coalesce with the jet. As a result the jet splits into two branches surrounding the cyclonic eddy. The two recirculating gyres are divided by the ridge and have shorter zonal length than do those in the no-ridge case. These specific flow patterns are observed in the Gulf Stream in the vicinity of the New England Seamount Chain and the Kuroshio over the Shatsky Rise.

1. Introduction

The purpose of this paper is to study influences of a submarine ridge on a strong oceanic jet using a simple numerical model. We pay special attention to the influences of the ridge on unsteady flow patterns of the jet, and observe whether meanders grow more rapidly, whether detached eddies are intensified, and whether the jet has a different pattern compared with the mesoscale features that occur in the same unstable jet when the ridge is not present.

In real oceans, there are several regions in which strong ocean currents cross over submarine ridges and have unsteady meanders and detached eddies. Some examples are the Gulf Stream over the New England Seamount Chain, the Kuroshio over the Shatsky Rise and the Emperor Seamount Chain, and the Antarctic Circumpolar Current in Drake Passage. There should be significant differences in flow properties in these regions as compared with those associated with the Gulf Stream flowing over a nearly flat bottom, east of Cape Hatteras and west of the New England Seamount Chain far away enough not to be influenced by the Chain.

---

[1]Contribution No. 521 from NOAA PMEL

From the Gulf Stream flowing over the nearly flat bottom, cyclonic eddies are detached southward, and anticyclonic eddies are detached northward. These eddies drift westward, and the Gulf Stream returns to the state of small-amplitude meanders after detachment. Amplitude of meanders, the number, distance, and strength of eddies, and zonal location of detachment are similar on the north and south of the Gulf Stream.

In the regions where the strong currents cross over the submarine ridges, some specific flow patterns have been observed, which have not been observed in the Gulf Stream over the flat bottom. Using satellite infrared images, Richardson (1981) suggested that the Gulf Stream had a cyclonic "ring-meander" south of the Gulf Stream axis, and that the eastern part of the ring-meander was located over the New England Seamount Chain. Another anticyclonic meander occurred north of the axis and immediately east of the Chain. Richardson noted that this feature was a common one appearing in several satellite images. Free drifting buoys which measured surface currents confirmed these cyclonic and anticyclonic motions at the same time as the satellite images. The flow pattern is schematically shown in figure 1, which is also typical of the Kuroshio around the Shatsky Rise as shown later. It may be a reasonable assumption that the Gulf Stream splits into two branches around the Seamount Chain.

Contour lines of 10°C-isotherm depth observed by Emery, Ebbesmeyer, and Dugan (1980) show that the Kuroshio splits into two branches surrounding a cyclonic eddy whose location relative to the Shatsky Rise was similar to the eddy around the New England Seamount Chain, although they did not mention the splitting. Monthly maps of temperature at 300-m depth made by Bernstein and White (1981) also show the splitting of the Kuroshio in the vicinity of the Shatsky Rise. These two eddies were confirmed by surface buoys, one of which drifted into the Kuroshio from the continental slope south of Japan and was trapped in the cyclonic eddy on the southern side of the main flow. The other traced along the northern edge of the anticyclonic eddy (Ishii, 1982). Gordon, Georgi, and Taylor (1977) observed that the Antarctic Circumpolar Current split into two branches west of the North Scotia Ridge in Drake Passage, although eddies were not clearly observed.

Although Richardson (1981) insisted that the flow pattern shown in figure 1 is semipermanent, there is still a question whether the pattern is permanent or not permanent but very frequent.

The mean temperature field at a depth of 450 m observed by Richardson (1980) shows that the New England Seamount Chain and Newfoundland Ridge break the circulation south of the Gulf Stream into three partially connected gyres.

Roden (1977) noted the differences in the strength of the perturbations of the Kuroshio between the western and eastern sides of the Emperor Seamount Chain, with the stronger in the west. In this region, however, specific flow patterns, such as jet splitting, which indicate the strong influence of bottom topography, have never been observed.

The numerical model chosen for the present study is similar to that of Ikeda and Apel (1981), in which meanders grow in an eastward-flowing jet because of instability, and eddies are detached from the large-amplitude meanders. The only difference is that the present model has a submarine ridge around the point where eddies are detached in the no-ridge case.

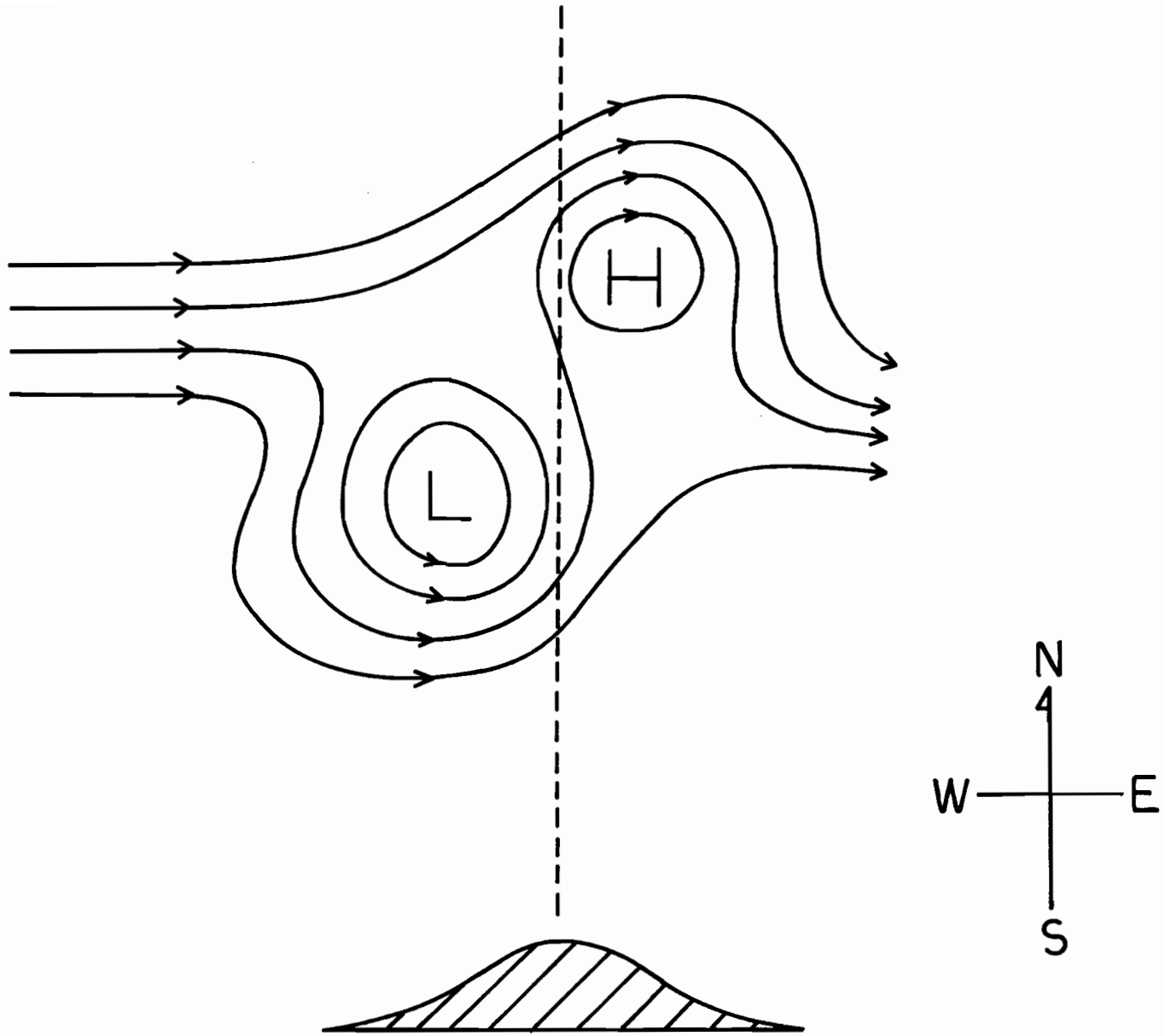

Figure 1. The streamlines schematically describe the flow patterns observed in the Gulf Stream around the New England Seamount Chain and in the Kuroshio around the Shatsky Rise. The bottom topography is shown by the side view of the general feature representing the Seamount Chain and the Rise.

We use a two-layer quasi-geostrophic model. The basic equations are those governing conservation of potential vorticity on a β-plane. An initial condition is that, in the upper layer, an eastward-flowing jet has meanders of one wavelength; that is, an initial streamline has one maximum and one minimum in the western side of the jet, where the distance between two extremes is similar to half the wavelength of the fastest growing linear solution. The lower layer is quiescent only in the initial state. As calculation time advances, meanders grow and propagate eastward in the integration domain whose zonal length is approximately six wavelengths. Then, the jet acquires large-amplitude meanders in the intermediate region between the western and eastern boundaries. The submarine ridge is assumed to extend north and south in the intermediate region. Since the lower layer moves because of momentum transport from the upper layer, the fluid feels the bottom topography. Hence, the meanders and eddies are influenced by the ridge.

The initial condition is justified, especially in terms of the relative location between the initial meanders and the ridge. The mean path of the Gulf Stream departs from the coast at Cape Hatteras (75°W) and crosses over the New England Seamount Chain at 63°W (Richardson, 1980). Many observations have shown that small-amplitude meanders grow to generate detached eddies approximately at 66°W and in the more eastern side (Hansen, 1970; Robinson et al. 1974; Ikeda and Apel, 1981). In other words, the Gulf Stream is not always disturbed to the point of eddy generation in the upstream side of the Seamount Chain, but alternatively has a relatively calm situation with small-amplitude meanders and a highly disturbed situation resulting in eddy generation. Therefore, the initial condition reasonably describes the Gulf Stream at the moment when small-amplitude meanders start to grow.

The Kuroshio departs from the continental slope at 140°E and crosses over the Shatsky Rise at 158°E (Bernstein and White, 1981). The distance between them is similar to that between Cape Hatteras and the New England Seamount Chain. The Kuroshio generally has larger-amplitude meanders west of the Shatsky Rise than does the Gulf Stream west of the Seamount Chain. The Kuroshio is always highly disturbed in the region east of the Shatsky Rise and west of the Emperor Seamount Chain. Since the Antarctic Circumpolar Current has no topography that restricts a path to a weakly disturbed situation near upstream of the North Scotia Ridge, the Current is always highly disturbed (Gordon et al., 1977). Therefore, the present model is capable of describing best the Gulf Stream and the Kuroshio around the Shatsky Rise well, but only poorly the Kuroshio around the Emperor Seamount Chain and the Antarctic Circumpolar Current.

Theory based on a steady state cannot explain the flow pattern mentioned above. According to the steady-state theory, streamlines are deflected toward the equator over a ridge and form stationary Rossby waves downstream. This pattern is inconsistent with the cyclonic ring (or meander) upstream of the ridge.

The model used by Huppert and Bryan (1976) differs from the present one in that they used a multilayer model, and they assumed bottom topography modeled after a seamount. The major difference, however, is in the classical hypotheses that a uniform parallel flow is perturbed by the bottom topography to have unsteady patterns. Their numerical experiments started from

a state of rest. A flow was forced by the uniform transport over a short time, and then, a nearly uniform flow felt the bottom and generated a perturbation. Therefore, if all parameters were fixed, only one flow pattern could appear.

By contrast, the flow in the present study is unstable and initially perturbed. The lower layer is set in motion by momentum transport from the upper layer and feels bottom topography. The bottom influences are dependent on relative locations between the ridge and meanders or eddies; that is, many different flow patterns can appear depending on relative locations between the ridge and the initial meanders. The model in the present study is more appropriate for describing the influences of a submarine ridge on a strong current, for example, the New England Seamount Chain on the Gulf Stream, and the Shatsky Rise on the Kuroshio.

For the purpose of representing all relative locations of the initial disturbance well enough, we make numerical calculations for four cases, taking into consideration both the reflection of the initial streamlines about the jet axis and the shift of a ridge location by approximately one-fourth of the meander wavelength.

In section 2, we outline the basic equations, the ridge location, the initial and boundary conditions, and numerical method. In section 3, flow patterns for the four cases are shown, compared with the flow pattern in the no-ridge case. In section 4, we present methods used for interpretation of the flow patterns--a map of vorticity induced by bottom topography, energy transfers among zonal Fourier components, etc. In section 5, the topographic effects on the flow patterns are estimated using the methods presented in section 4. In section 6, a parameter study is performed with the variations of the ridge height and width. In section 7, numerical results are compared with specific flow patterns observed in the Gulf Stream around the New England Seamount Chain, the Kuroshio over the Shatsky Rise, and the Antarctic Circumpolar Current in Drake Passage.

2. Basic Equations, Ridge Locations, Initial and Boundary Conditions, and Numerical Method

The basic equations used are those governing conservation of potential vorticity in a two-layer quasi-geostrophic flow as

$$\frac{D_1}{Dt}\left(\nabla_H^2 p_1 + by + \frac{\eta}{d}\right) = 0, \qquad (2.1)$$

$$\frac{D_2}{Dt}\left(\nabla_H^2 p_2 + by + \frac{h-\eta}{1-d}\right) = 0,$$

and

$$\eta = F(p_2 - p_1),$$

where

$$D_j/Dt = \partial/\partial t + \vec{v}_j \cdot \mathrm{grad}, \quad (j = 1, 2)$$

$$\nabla_H^2 = \partial^2/\partial x^2 + \partial^2/\partial y^2,$$

and

$$\vec{v}_j = (-\partial p_j/\partial y,\ \partial p_j/\partial x).$$

The coordinates x and y are eastward and northward, respectively, and t is the time, p is the pressure, which is identical to a stream function in the quasi-geostrophic approximation. The suffixes 1 and 2 denote the upper layer and the lower layer, respectively. The interface between the two layers is assumed to be

$$-d + \varepsilon\eta,$$

and the bottom topography is represented by

$$-1 + \varepsilon h,$$

where $\varepsilon = U/(f_o\bar{L})$ is a Rossby number.

The nondimensional parameters in the basic equations (2.1) are chosen in the following way. A ratio of the upper-layer thickness to the total fluid depth, $d = D/\bar{H}$, is 0.3, where the interface between the two layers is analogous to the main thermocline. An internal rotational Froude number, $F = f_o^2\bar{L}^2/(g'\bar{H},)$ is 1, where $g' = g\Delta\rho/\rho_o$ is the reduced gravitational acceleration, f_o is the Coriolis parameter at $y = 0$, and $\bar{L}$ is the horizontal length scale, a half-width of the jet. The β-plane parameter, $b = \beta\bar{L}^2/U$, is 0.1, where U is the velocity scale, a maximum speed of the initial jet. The time scale is $\bar{L}/U$. An internal Rossby radius of deformation is $(d(1-d)/F)^{\frac{1}{2}} = 0.46$.

The scales referred to the Gulf Stream are $\bar{H}$ = 4 km, D = 1 km, $g' = 10^{-2}$ m s^{-2}, $f_o = 10^{-4}$ s^{-1}, $\beta = 1.6 \times 10^{-11}$ m^{-1} s^{-1}, $\bar{L}$ = 60 km and U = 1 m s^{-1}, where $\bar{L}$ and U are determined so that the velocity profile of the basic jet may represent the Gulf Stream at a depth of 500 m, the mid-depth between the sea surface and the main thermocline. The nondimensional parameters are $\varepsilon = 0.17$, $d = 0.25$, $F = 0.9$ and $b = 0.06$. Although there are differences between the values chosen in the present paper and the values referred to the Gulf Stream, it has been confirmed by Ikeda and Apel (1981) that there is no difference in the essential properties; that is, eddies are detached from the jet, and two recirculating gyres are generated on the northern and southern sides of the jet. Therefore, the model represents the Gulf Stream and the Kuroshio well.

The bottom topography is assumed to be

$$h = h_o \exp\{-0.5(x-x_R)^2/\ell^2\}\ , \qquad (2.2)$$

which denotes the north-south extending ridge whose summit is located at $x = x_R$. h_o is the height, and ℓ denotes the width. For the purpose of including the variations of the relative locations between the ridge and the initial meanders, x_R is chosen as

$$x = 12.5 \text{ or } 13.5$$

with the variation of 1, where the domain of numerical calculations is taken to be $0 < x < 27$. It is mentioned below that this variation corresponds to one-fourth of the meander wavelength.

The initial state is taken as the total stream function, which has the form

$$p_1 = p_{1B} + p_A(x - 3)\exp\{-0.5(x - 3)^2 - y^2\},$$
$$p_2 = 0, \tag{2.3}$$

for the upper layer and the lower layer, respectively, where the basic flow consists of an eastward jet in the upper layer with a Gaussian velocity profile described by

$$p_{1B} = -\int_0^y \exp(-y^2)dy.$$

The initial state indicates that a localized perturbation is superimposed on the basic jet in the form of a single wave centered at (3, 0). In contrast, the lower layer is quiescent at $t = 0$. The value of p_A is chosen as

$$p_A = 0.1 \text{ or } -0.1.$$

When p_A is chosen to be 0.1, a streamline of $p_1 = 0$ has a minimum of $y = -0.1\ e^{-\frac{1}{2}}$ at $x = 2$ and a maximum of $y = 0.1\ e^{-\frac{1}{2}}$ at $x = 4$. In the case of $p_A = 0.1$, the streamline has a maximum at $x = 2$ and a minimum at $x = 4$; that is, the streamline is reflected about the jet axis, which is identical to a meander shift by a half wavelength.

We mention length scales associated with perturbations, and the relationship with the ridge width and the variations of the ridge location. According to Ikeda and Apel (1981), in which the no-ridge case was studied, the fastest growing solution has a wavelength of 4.5 at least before an eddy is detached. Diameters of detached eddies are 1.8, which is of the same order as half the ridge width, $1.4\ (=1/0.5)^{\frac{1}{2}}$ determined by (2.2) for $\ell = 1$. By selecting the values of x_R and p_A, we make four cases among which the relative locations of meanders to the ridge vary at intervals of approximately one-fourth of the wavelength, because the relative locations shift by approximately one-fourth with the variation of x_R, and by a half with the change of p_A. These four cases, A, B, C, and D, are presented in table 1, together with the no-ridge case N, where the ridge shape is fixed as $h_o = 1$ and $\ell = 1$.

In addition to the variations of the relative locations between the ridge and the initial meanders, the ridge shape is varied as

$$h_o = 1 \text{ or } 0.5,$$

and

$$\ell = 1 \text{ or } 0.5.$$

where h_o denotes the height, and $2^{\frac{1}{2}}\ell$ denotes the half width at which $h = h_o e^{-1}$. With the pivot at $h_o = 1$ and $\ell = 1$, numerical calculations are performed for two cases, DH and DW, shown in table 2. The initial condition and the ridge

Table 1. The four cases (A, B, C, and D) in which the submarine ridges are assumed to exist and one case (N) without a ridge.*

Case	x_R	p_A	θ_A
A	12.5	0.1	0°
B	12.5	-0.1	±180°
C	13.5	0.1	-90°
D	13.5	-0.1	+90°
N	----	0.1	----

*The ridge-summit location is denoted by x_R in (2.2) which indicates the bottom topography. p_A denotes shapes of the initial streamlines given by (2.3). The phase difference, θ_A, denotes the eastward advances of meanders compared with case A, where 360° corresponds to one wavelength.

Table 2. One basic case (D) and two cases (DH and DW) by which effects of the ridge height and width are examined.*

Case	h_o	ℓ
D	1	1
DH	0.5	1
DW	1	0.5

*The height is determined by εh_o, and the half width by $2^{\frac{1}{2}}\ell$ in (2.2), where ε is a Rossby number. The initial condition determined by p_A (=-0.1) and the ridge location by x_R (=13.5) are the same as case D.

location are the same as in case D, because the most typical effects of the ridge appear in case D compared with cases A through C, as shown in Section 3.

Based on the scales, $H = 4$ km, $\bar{L} = 60$ km and $\varepsilon = 0.17$, the pivot ($h_0 = 1$, $\ell = 1$) corresponds to the height of 680 m ($\varepsilon h_0/H = 0.17$) and the half width of 88 km. The Shatsky Rise has a height as $\varepsilon h_0/H = 1500$ m/5000 m and a half width of 100 km, approximately. It is difficult to estimate the effective shape of the New England Seamount Chain, because the Seamount Chain is composed of several peaks whose horizontal scales are tens of kilometers. However, it is clear that the Seamount Chain is narrower than the Shatsky Rise.

The calculation domain has two open boundaries on the west and east. On the western (upstream) boundary, x-derivatives of the pressure and potential vorticity are assumed to be zero to avoid oblique streamlines on the boundary. On the eastern (downstream) boundary, the pressure and potential vorticity are fixed until $t = 30$, and they are assumed to propagate through the boundary at a given speed, $c_D = 0.15$, after $t = 30$, because a significant perturbation reaches there immediately after $t = 30$. The value of c_D is selected to be identical to the phase velocity of the meanders appearing in the vicinity of the downstream boundary similarly to Ikeda and Apel (1981). It has been confirmed that those boundary conditions make no serious deformation of flow in the intermediate region where eddies are detached and influenced by the ridge. The northern and southern boundaries are slippery walls on which the perpendicular velocity vanishes.

The numerical method is identical to one used in Ikeda (1981). We convert the basic equations to the finite-difference equations. The finite-difference scheme used has no artificial viscosity due to upstream differences. However, smoothing is performed at $t = 30$ and 36, since it is needed for the suppression of local instability caused by the numerical scheme. By smoothing, the potential vorticity at each calculating point is replaced by an average of five points, including the point itself and the four points nearest to it. The solutions obtained using this scheme have been confirmed to describe jet meanders and detached eddies by Ikeda (1981).

3. Flow Patterns

The time variations of the p_1-contour lines, which are identical to the stream function in the upper layer, are shown in figure 2 at $t = 24$, 30, 36, and 42 for cases N, A, B, C, and D. All meanders are marked by 'm' and are numbered sequentially from west to east. The location of a meander is defined as the position of a maximum or minimum in the contour line for which $p_1 = 0$. The meanders, m_0 and m_1, correspond to two extremes of the initial jet.

We briefly describe the evolution in the no-ridge case N. All meanders propagate eastward (downstream) and grow, keeping in proper order until $t = 24$, although the flow patterns are not shown before $t = 24$. Then, between $t = 24$ and $t = 30$, the three meanders, m_0, m_1, and m_2, interact with each other; that is, m_0 overtakes m_2. After the overtaking, a cyclonic eddy, E_2, is detached southward, and a new meander, M_2, forms. The new meander M_2

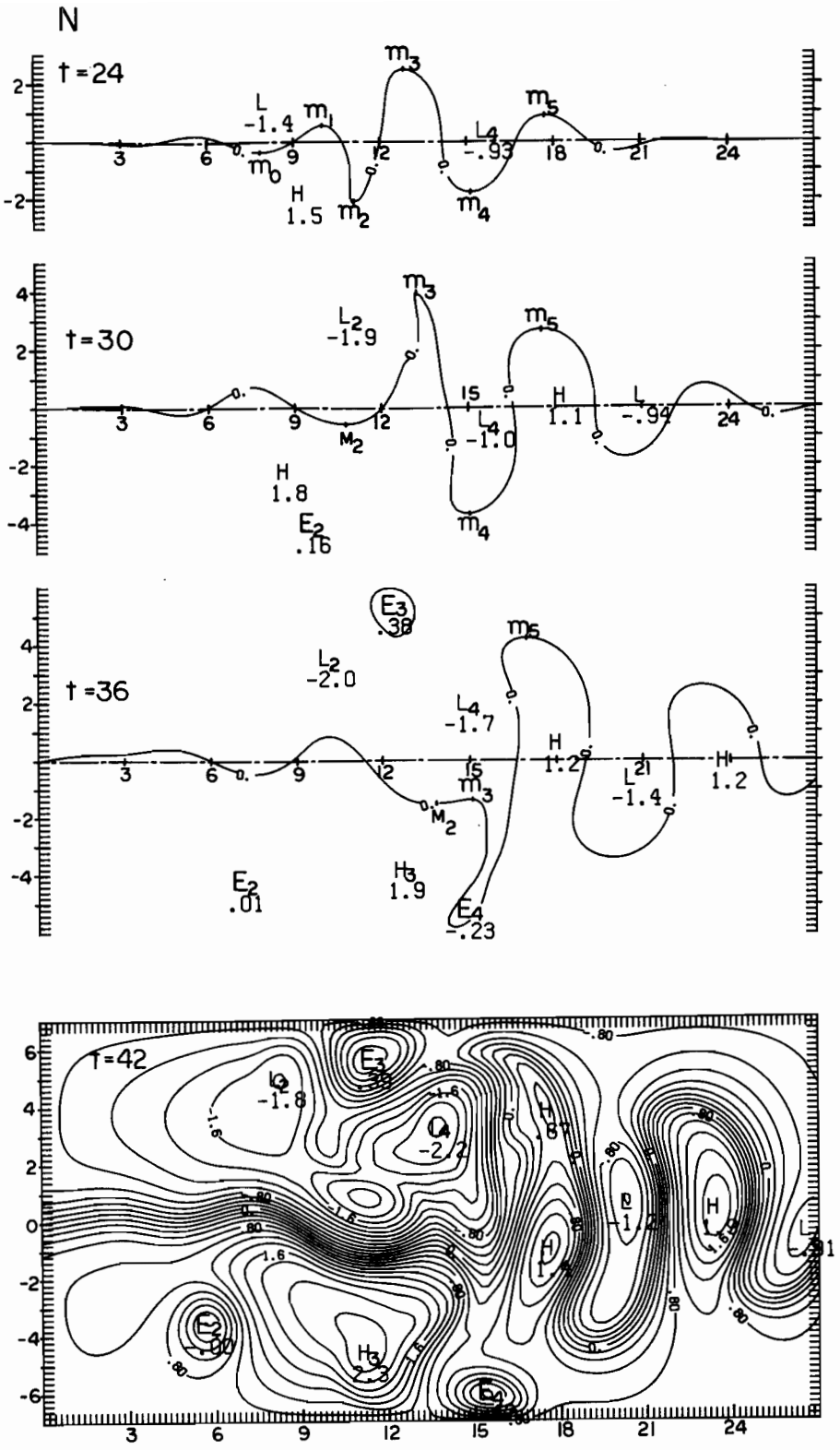

2a.

Figure 2. The time variations of the upper-layer stream function with only $p_1 = 0$ shown at t = 24, t = 30, and t = 36. 'm' and 'E' denote a meander and a detached eddy, respectively. Capital 'M' denotes a new one generated after meader interactions. Cases (a) N, (b) A, (c) B, (d) C, and (e) D are listed in table 1. E_2' of cases A and D are generated after E_2 is detached from m_2. The bottom topography is shown by the side view of the ridge in each figure, and the summits are indicated by broken lines.

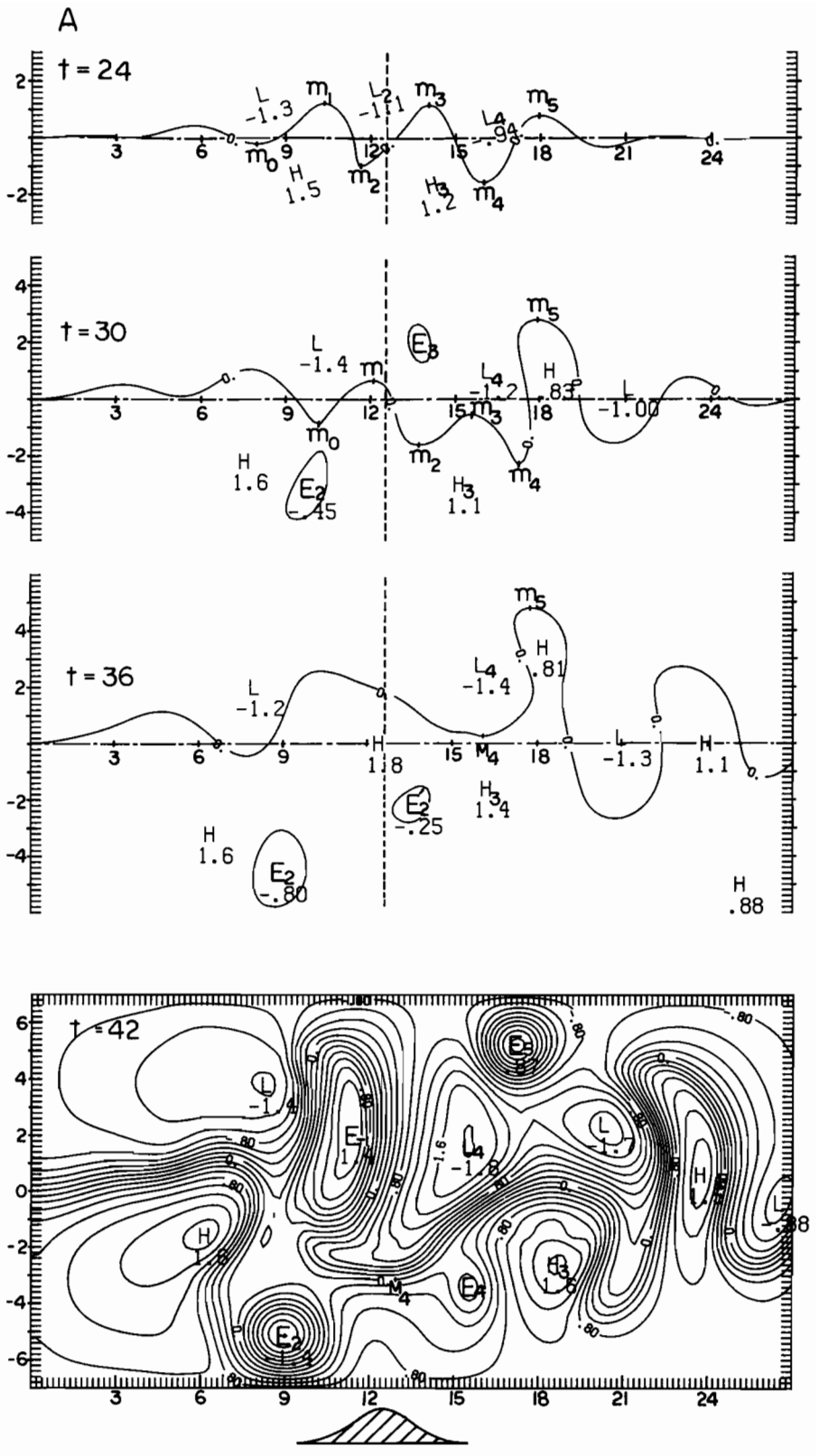

2b.

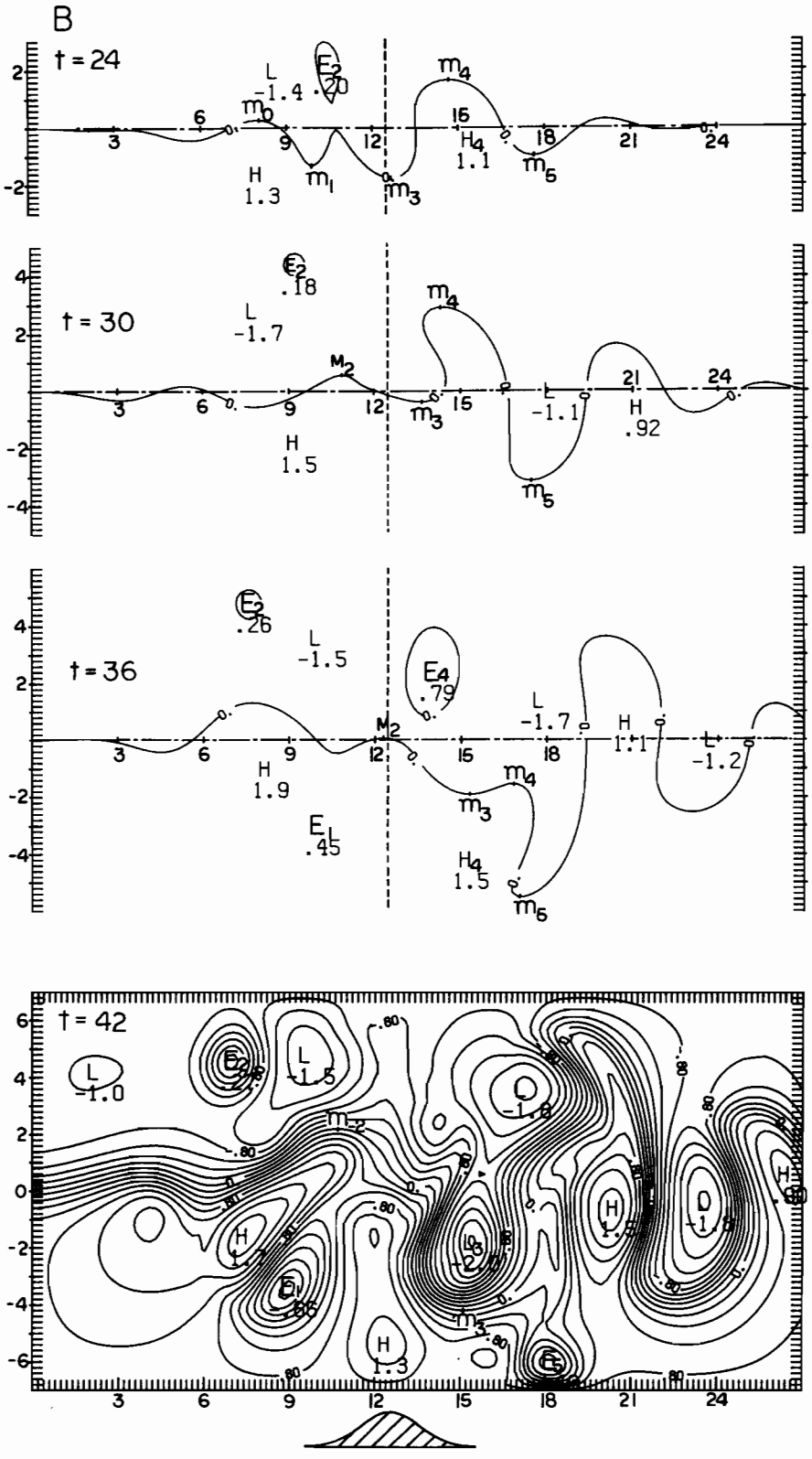

2c.

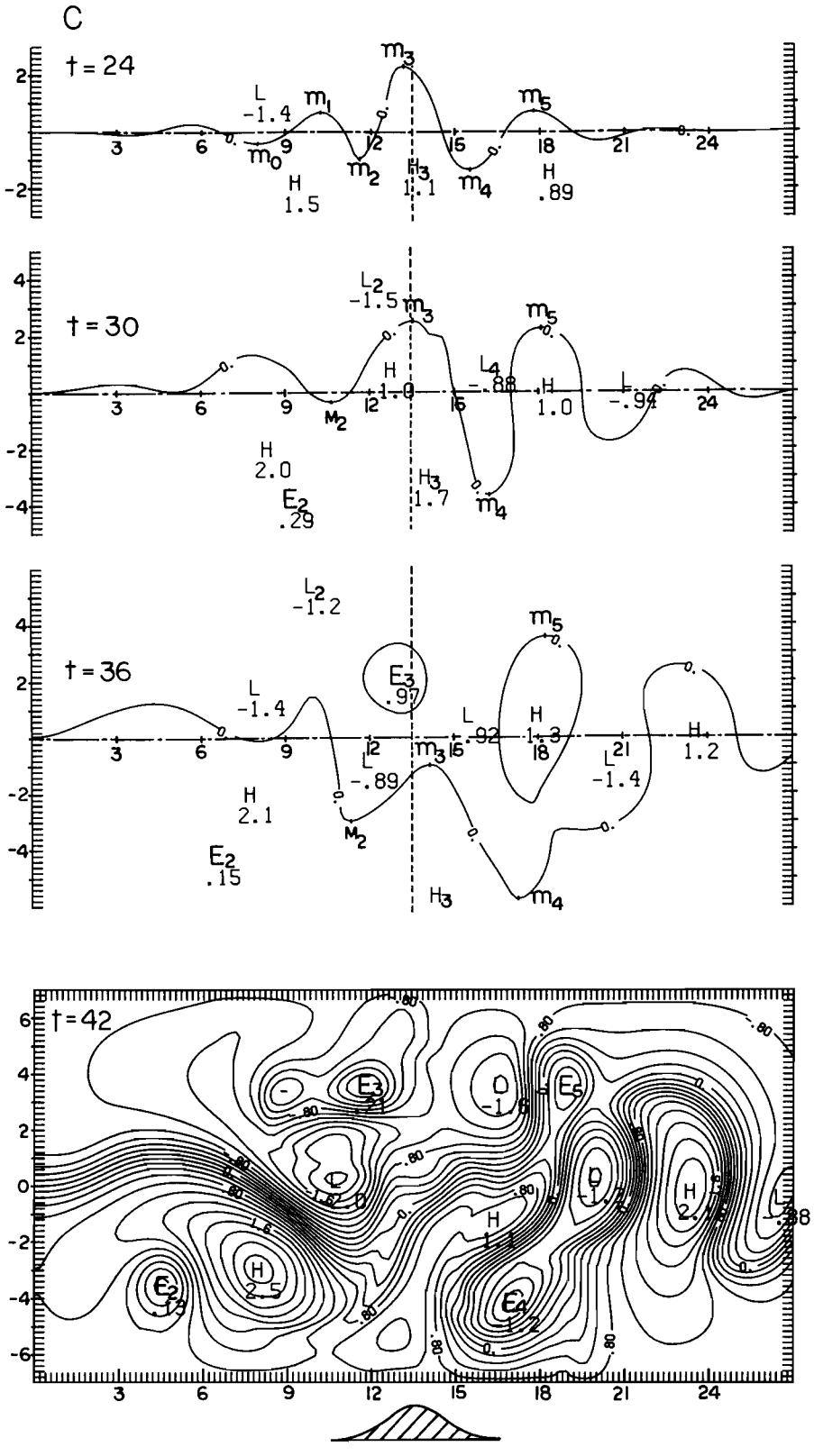

2d.

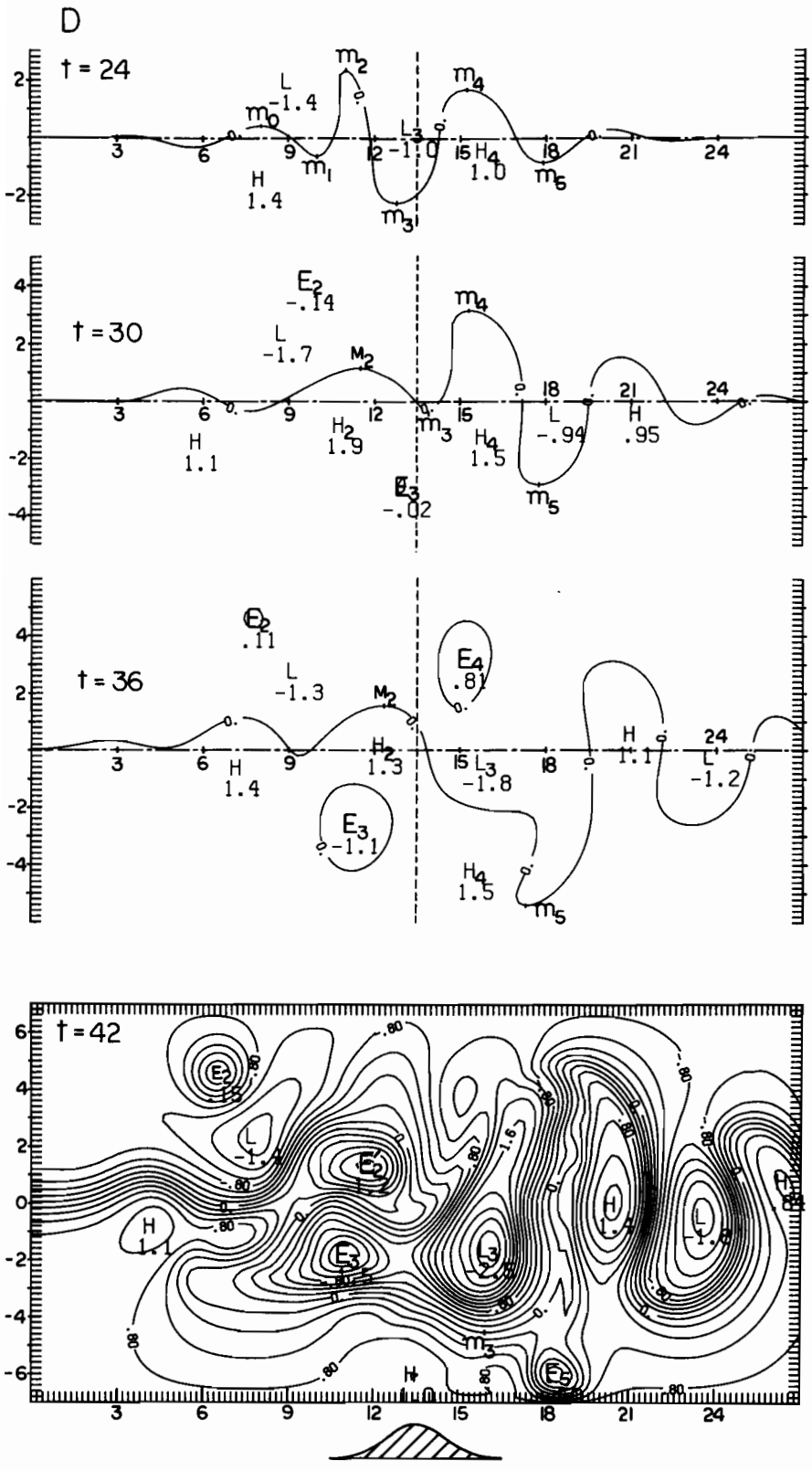

2e.

propagates very fast and overtakes m_3 and m_4. Subsequent to this overtaking, an anticyclonic eddy, E_3, is detached northward from m_3 between t = 30 and t = 36, and a cyclonic eddy, E_4, is detached southward from m_4 between t = 36 and t = 42. The state of a small-amplitude motion is established at least at x < 15 after the eddy detachment, and two large-scale recirculating gyres form north and south of the jet flowing nearly zonally.

Let us look at the flow patterns for the ridge cases. If there were no ridge in cases A, B, C, and D, the patterns in cases A and C would be identical to those in the no-ridge case N, and cases B and D would have patterns reflected about the x-axis from those of case N with the change of sign of p_1. Although no pattern is shown, there is no significant difference between the patterns of the no-ridge case and the ridge cases until t = 18, except for the reflection in cases B and D. The reason is that flows are weak in the lower layer in the vicinity of the ridge.

In contrast, for t > 24, as meanders grow and propagate eastward, the lower layer moves and feels the bottom topography, which results in differences caused by the ridge. Table 3 shows the maximum strength of pressure anomalies in the eddies, when and at what y-location the eddies are detached, and whether the eddies coalesce with the major jet. From the flow patterns shown in figure 2 and the eddy features in table 3, it is first

Table 3. The features of the detached eddies.*

	N	A	B	C	D
E_2	L, 0.0 26, -4 no	L, -1.4 26, -3 no	H, +0.3 22, +5 no	L, +0.1 26, -4 no	H, +0.2 23, +4 no
E_3	H, +0.4 31, +5 no	H, +0.1 26, +3 yes		H, +1.0 32, +2 no	L, -1.5 28, -3 yes
E_4	L, -0.4 36, -6 no	L, -0.1 32, -4 no	H, +0.8 32, +3 yes	L, -1.2 40, -5 --	H, +0.8 32, +3 yes
E_5	H, -- 42, >+6 no	H, +0.9 36, +4 no	L, -0.5 36, -5 no	H, +0.3 40, +4 --	L, -0.5 36, -5 no

*Five items in each matrix element denote the kind of pressure anomaly, the maximum strength, the detachment time, the detachment y-location, and whether the eddy coalesces with the major jet. -- denotes that it is unclear in the present calculations.

noticed that there are large differences among the four ridge cases. In other words, the flow evolution strongly depends on the relative locations of meanders to the ridge. We can see the following examples: no meander overtakes until t = 30 in case A, while m_0 overtakes m_2 in all other cases. No eddy is generated from m_3 in case B, but E_3 is detached in case D. Especially, the patterns at t = 42 look very different among the four cases.

Although there are many differences among the ridge cases, we find behaviors that are common in some of the ridge cases and significantly different from those of the no-ridge case. Some of them, however, appear only under special conditions; for example, no stronger eddy exists south of the jet on the western slope in case C, unlike all other cases. The common behaviors are summarized below with all examples shown in table 4.

1. Eddies are detached more rapidly than in the no-ridge case.
2. Eddies are detached closer to the region of the jet axis than in the no-ridge case.
3. Detached, cyclonic eddies are strengthened south of the jet on the western slope of the ridge, and anticyclonic eddies are strengthened north of the jet on the eastern slope.
4. The jet meanders northward over the western slope, on which a high-pressure anomaly exists, and meanders southward over the eastern slope, with a low-pressure anomaly.
5. A detached, cyclonic eddy travels northward on the western slope and coalesces with the jet, and anticyclonic eddies coalesce with the jet traveling southward on the eastern slope.
6. The jet splits into two branches.
7. Each recirculating gyre is divided into two parts, one west and one east of the ridge.

We examine the mechanisms by which the flows have these behaviors, considering effects of the bottom topography in section 5.

4. Method of Examining Topographic Effects

4.1 Balance of Vorticity

By the integration of the basic equations (2.1) with respect to z through each layer, we have

$$\frac{D_1}{Dt} d\nabla_H^2 p_1 + bdv_1 + \frac{D_1\eta}{Dt} = 0,$$
$$\frac{D_2}{Dt} (1-d)\nabla_H^2 p_2 + b(1-d)v_2 + u_2\frac{\partial h}{\partial x} - \frac{D_2\eta}{Dt} = 0. \qquad (4.1)$$

The second equation in (4.1) indicates that bottom topography influences the relative vorticity in the lower layer, $\nabla_H^2 p_2$, through the term $u_2 \partial h/\partial x$. If

Table 4. The common behaviors in the ridge cases and examples of them.

		A	B	C	D
1.	more rapid detachment	E_3, E_4, E_5	E_4, E_5		E_3, E_4, E_5
2.	closer to axis	E_3, E_4, E_5	E_4, E_5	E_3, E_4, E_5	E_3, E_4, E_5
3.	stronger				
	south-west	E_2	E_1		E_3
	north-east		E_4		E_4
4.	meander				
	middle-west	E_{-1}	m_{-2}	E_3	$*E_2'(M_2)$
	middle-east	M_4	m_3		m_3
5.	coalescence				
	south-west				E_3
	north-east	E_3	E_4		E_4
6.	jet splitting	no	no	no	t = 42
7.	gyre divisions	yes	yes	yes	yes

NOTE: * E_2' denotes the second eddy generated from M_2 after E_2 is detached from m_2.

there is some mechanism by which one layer tends to move in the same way as the other, then $\nabla_H^2 p_1$ is also influenced by the bottom topography. A positive $(-u_2 \partial h/\partial x)$ generates an increase in the relative vorticity, which corresponds to a low-pressure anomaly. Hence, the simplest method of examining topographic effects qualitatively is to compare a map of $(-u_2 \partial h/\partial x)$ with locations of pressure anomalies.

In order to estimate the strength of the topographic effects quantitatively, integrating (4.1) with respect to x and t in a concerned region and time, we obtain

$$\begin{aligned} RV1 + IH1 &= AD1 + AB1 + AP1, \\ RV2 + IH2 &= AD2 + AB2 + AT + AP2, \end{aligned} \tag{4.2}$$

where

$$\begin{aligned} RVj &= d_j \iint \frac{\partial}{\partial t} \nabla_H^2 p_j \, dx \, dt, \\ ADj &= -d_j \iint \vec{v}_j \cdot \mathrm{grad} \nabla_H^2 p_j \, dx \, dt, \\ ABj &= -b d_j \iint v_j \, dx \, dt, \\ IH1 &= -IH2 = -\iint \frac{\partial \eta}{\partial t} \, dx \, dt, \\ AP1 &= -AP2 = -\iint \vec{v}_j \cdot \mathrm{grad}\, \eta \, dx \, dt, \\ AT &= -\iint u_2 \frac{\partial h}{\partial x} \, dx \, dt, \\ d_1 &= d, \text{ and } d_2 = 1 - d. \end{aligned}$$

The equations (4.2) describe the following budgets of potential vorticity: both the relative vorticity, whose time variation is denoted by RVj, and the interface height, whose variation is denoted by IH1 (= -IH2), are induced by advections of these two quantities, ADj and APj, and the meridional variation of a Coriolis term, whose contribution is denoted by ABj, plus the stretching of a vortex pole because of the bottom topography, AT, in the lower layer.

The topographic effects are estimated in the following way: under the condition that ABj is negligible compared with the other terms, AT induces RV2-AD2 and IH2-AP2, which is identical to -(IH1-AP1) and nearly equal to RV1-AD1. In other words, the bottom topography contributes the variation of the relative vorticities in the lower layer, RV2-AD2, and also in the upper layer, RV1-AD1, through the variation of the interface height. These two terms are compared with the advection terms, ADj.

When the variation of the interface height, IH1-AP1, dominates over AT and is a major source of generation of the vorticity, the above estimation is unreasonable. In this case, however, it is clear that the bottom effects are minor.

4.2 Energy Transfers among Zonal Fourier Components

The present method of Fourier analysis is similar to that proposed by Ikeda and Apel (1981). The steady basic jet whose profile is represented by $p_1 = -\int_o^y \exp(-y^2)dy$ and $p_2 = 0$ is assumed to exist in the regions where $-\infty < x < 0$ and where $27 < x < \infty$. Strictly speaking, this assumption is reasonable only when the pressure and potential vorticity are fixed on the western and eastern boundaries. However, since these values vary slightly even for $30 < t < 36$, the assumption is reasonable.

Under that assumption, all flow quantities and bottom topography are represented by Fourier transforms with respect to zonal wavenumber k. For example,

$$p_j\ (x,\ y,\ t) \ = \ \int_{-\infty}^{\infty} \tilde{p}_j(k,\ y,\ t)\ \exp(ikx)dk, \tag{4.3}$$

where

$$\tilde{p}_j(k,\ y,\ t) = \frac{1}{2\pi}\int_{-\infty}^{\infty} p_j(x,\ y,\ t)\ \exp(ikx)dx. \tag{4.4}$$

The component, $\tilde{p}_j(-k)$, which has negative wavenumber k is identical to the complex conjugate of $\tilde{p}_j(-k)$;

$$\tilde{p}_j(-k) = \tilde{p}_j{}^*(k).$$

The negative-wavenumber components are used to simplify Fourier analysis.

The total energy, E, is composed of kinetic energy in each layer and potential energy associated with the interface height. The total energy is represented as an integral of energy associated with Fourier components as

$$E = \int_{-\infty}^{\infty} \tilde{E}(k)dk. \tag{4.5}$$

The time variation of $\tilde{E}(k)$ is contributed by the other components. The contributions are divided into two parts. One of them is the interaction between the component that represents the bottom topography with wavenumber k' and the component that represents the flow with wavenumber k - k'. Another is the interaction between the two flow-components with k' and k - k'. Substituting the Fourier transforms (4.3) for p_j in the basic equations (2.1), and multiplying resultant equations for the k component by $\tilde{p}_j{}^*(k)$, we obtain $\partial\tilde{E}(k)/\partial t$

$$\frac{\partial\tilde{E}(k)}{\partial t} = ET + EA, \tag{4.6}$$

where

$$ET = \int_{-\infty}^{\infty} \tilde{T} < k,\ k',\ k'' > dk',$$

$$EA = \int_{-\infty}^{\infty} \tilde{A} < k,\ k',\ k'' > dk',$$

$$\tilde{T} < k,\ k',\ k'' > = -2\pi Re\ [i\int_{-Y_o}^{Y_o} J_2(k,\ k'')\ \tilde{h}(k')\ dy], \tag{4.7}$$

$$J_2(k,\ k'') = k\tilde{p}_2{}^*(k)\ \partial\tilde{p}_2(k'')/\partial y + k''\tilde{p}_2(k'')\ \partial\tilde{p}_2{}^*(k)/\partial y,$$

k" is k - k', and Re denotes the real part. The two terms in the righthand side of (4.6) have the following meaning: $\tilde{T}$ < k, k', k" > denotes the energy transfer from the k" (= k - k') flow-component to the k flow-component caused by the interaction with the k' bottom-component. The total transfer to the k component is denoted by ET. $\tilde{A}$ < k, k', k" > denotes the transfer from the k' and k" flow-components caused by the interaction between these two components, and EA is the total transfer. The term EA, discussed by Ikeda and Apel (1981), has three forms of transfer: to and from kinetic energy in the upper layer or in the lower layer, and to and from potential energy. In the present study, we consider ET and the total EA; that is, the transfer caused by the bottom effects, and the transfer not caused by the bottom effects.

5. Mechanisms of Bottom Topographic Effects

Let us study the relationship between the ridge effects and the behaviors common to the ridge cases listed in table 4.

5.1 Eddy Generation Influenced by the Ridge

We first examine the behaviors shown in 1 to 4 of table 4. The behaviors 1 and 2 suggest that the ridge promotes eddy detachment; that is, eddies are detached from smaller-amplitude meanders than are those in the no-ridge case. All behaviors 1 to 4 show that the ridge promotes the generation of eddies which would be detached even if there were no ridge, and that the ridge generates eddies which would not be generated without the ridge.

5.1.1. Basic Concept of Vorticity Generation by the Ridge Effects on Recirculating Gyres

The basic concept is shown schematically in figure 3. The condition for this concept is that recirculating gyres are generated. As shown for case D in figure 4 gyres are generated in the northern and southern sides of the jet for x < 15 by the time t = 30. Although a typical bipolar shape of the gyres is not seen at t = 36, it is still correct that the lower layer has a region of eastward flow and two of westward flow north and south of it.

The positive $(-u_2 \partial h/\partial x)$ generates the positive relative vorticity, which corresponds to a low-pressure anomaly, while the negative $(-u_2 \partial h/\partial x)$ makes a high-pressure anomaly. Therefore, low- and high-pressure anomalies are generated in the westward flows on the western and eastern slopes of the ridge, respectively. In contrast, in the eastward flow, a high-pressure anomaly is generated on the western slope, and a low-pressure anomaly on the eastern slope.

If meanders and eddies encounter the special conditions proposed above, the meanders are easily cut off to form eddies, and the eddies are strengthened. To put it more concretely, northward meanders which exist on the

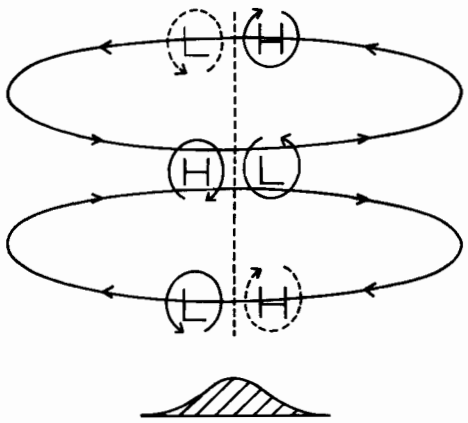

Figure 3. The basic concept is shown schematically. Pressure anomalies are generated by the ridge effects on the recirculating gyres.

westward flow of the gyres are easily cut off over the eastern slope, while southward meanders are easily cut off over the western slope. These phenomena are realized by behaviors 1 and 2 in table 4. The eddies listed in behavior 3 are examples of cyclonic eddies which are detached southward and strengthened on the westward flow over the western slope, and examples of anticyclonic eddies which are detached northward and strengthened on the westward flow over the eastern slope. As shown by behavior 4, the major jet which exists on the eastward flow of the gyres meanders northward over the western slope and southward over the eastern slope. Each case is discussed in the following subsections.

5.1.2. Case C

A map of $(-u_2 \partial h/\partial x)$ at $t = 30$ is shown in figure 5. Compared with the flow pattern at $t = 36$ shown in figure 2, the negative anomaly of $(-u_2 \partial h/\partial x)$ is located at the same position as the high-pressure anomaly of the anticyclonic detached eddy, E_3, located at (12.8, 2.2). This agreement indicates that E_3 is also strengthened in the upper layer because of the topographic effects.

We have found the correspondence between ridge effects and the eddy in the upper layer. Let us estimate a ratio of the topographic effects to the variations of the relative vorticity in the eddy, using (4.2) which are obtained from the basic equations being integrated with respect to x and t. We consider the region of $11.5 < x < 14.5$ which includes the eddy E_3 and the time $30 < t < 31$ during which E_3 is generated. Each term in (4.2) is plotted versus y in figure 6 except for ABj which is negligible. The physical meaning of each term is discussed in section 4.1.

a

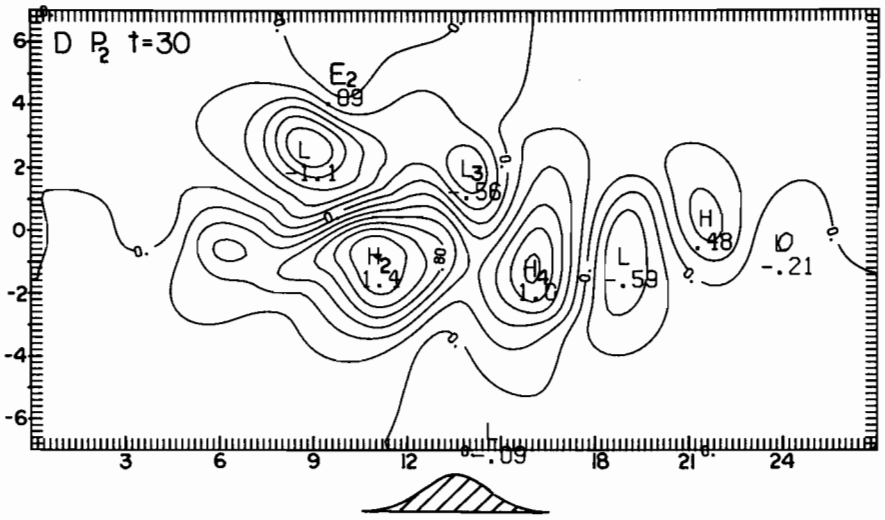

b

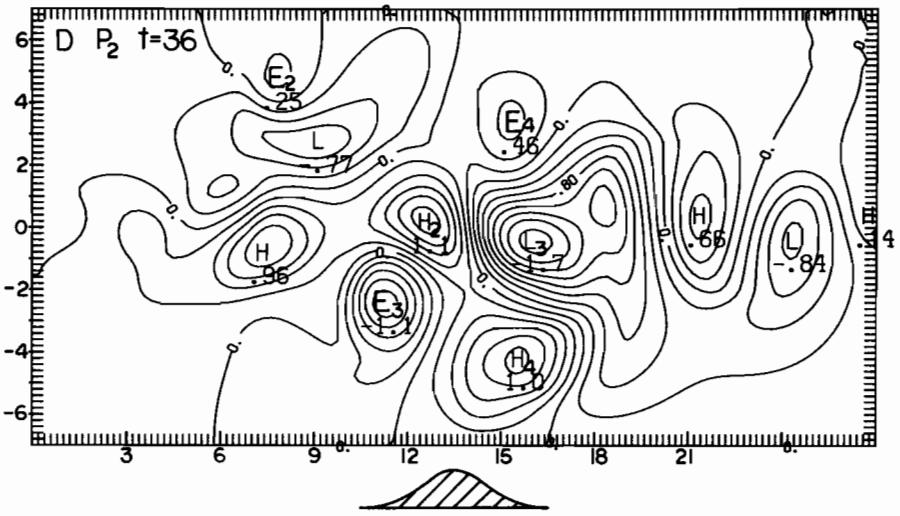

Figure 4. The lower-layer stream function of case D at (a) t = 30 and (b) t = 36.

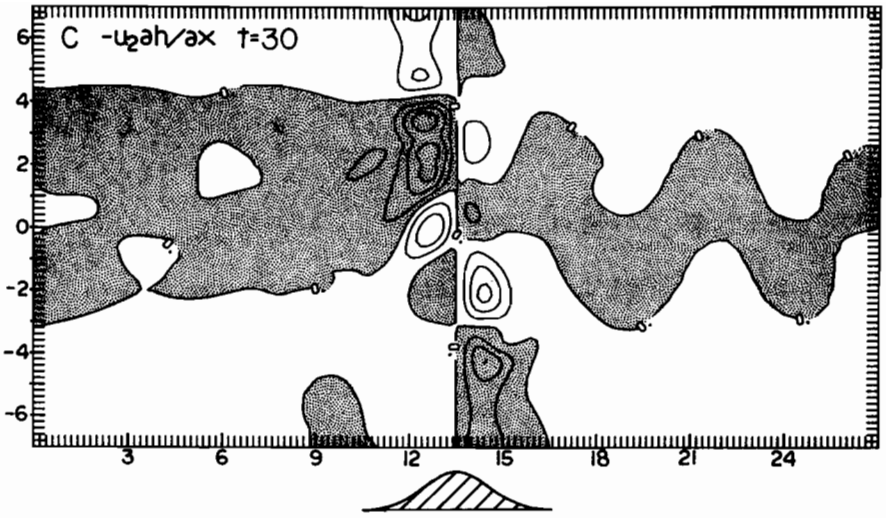

Figure 5. $(-u_2 \partial h/\partial x)$ at t = 30 of case C. Dotted area denotes the negative value. The topographic effects are compared with the flow pattern in the upper layer at t = 36 shown in figure 2.

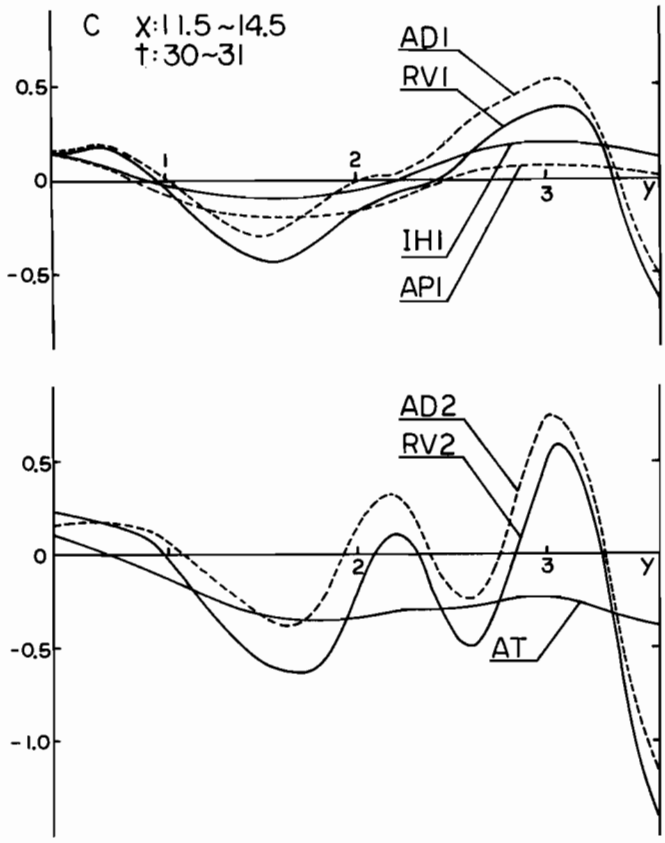

Figure 6. The balance of vorticity versus y integrated from x = 11.5 to x = 14.5 and from t = 30 to t = 31 for case C in (a) the upper layer and (b) the lower layer. All terms are discussed in section 4.2. ABj is not plotted, because it is negligible.

Around y = 2 at which E_3 is located, each term is roughly evaluated as

AT = -0.3, IH2 - AP2 = AP1 - IH1 = RV1 - AD1 = -0.1,

RV2 - AD2 = -0.2,

RV1 = -0.2, AD1 = -0.1, RV2 = -0.3, AD2 = -0.1.

These values are interpreted in the following way: the ridge effects denoted by AT are separated into the upper layer (RV1 AD1) by one-third and the lower layer (RV2 AD2) by two-thirds. The part affecting the upper layer contributes half of the variation of the relative vorticity (RV1) and has the same amount as the advection of the relative vorticity (AD1). The part affecting the lower layer has two-thirds of the variation of the relative vorticity (RV2). These budgets are represented by

$$AD1 \overset{-0.1}{\rightarrow} RV1 \overset{-0.1}{\leftarrow} AT \overset{-0.2}{\rightarrow} RV2 \overset{-0.1}{\leftarrow} AD2.$$

Since two detached eddies, E_4 and E_5, are located far enough from the ridge not to be affected, it is a reasonable interpretation that they are detached more rapidly because of indirect influences of the ridge; that is, the detachment point propagates downstream at higher speed compared with the no-ridge case.

5.1.3. Cases D, A, and B

We first study case D, and then conjecture an analogy for cases A and B on the basis of similar points in the flow patterns.

A map of $(-u_2 \partial h/\partial x)$ at t = 30 of case D is shown in figure 7, and compared with the flow patterns at t = 36 in figure 2. Although there are minor differences of locations, the positive anomalies of $(-u_2 \partial h/\partial x)$ correspond to the low-pressure anomalies associated with E_3 and m_3, and the negative anomalies to the high-pressure anomalies of E_4 and M_2. Also, in this case, as well as in case C, we observe the close agreement between the ridge effects and the pressure anomalies in the upper layer.

Since E_5 is far enough from the ridge, it is interpreted that the more rapid detachment of E_5 is due to indirect influences of the ridge like E_4 and E_5 in case C.

Let us examine the detailed mechanisms of intensification of E_3 and E_4 using (4.2). The vorticity balance for E_3 is shown in figure 8 for the region 11.7 < x < 13.9 and the time 30 < t < 31. As with E_3 of case C, the budgets are obtained as

$$AD1 \overset{0.0}{\rightarrow} RV1 \overset{0.1}{\leftarrow} AT \overset{0.3}{\rightarrow} RV2 \overset{0.2}{\leftarrow} AD2.$$

Since the transfers from AT to RVj dominate over those from Adj, it is concluded that the ridge effects are a major cause of the eddy intensification in both layers.

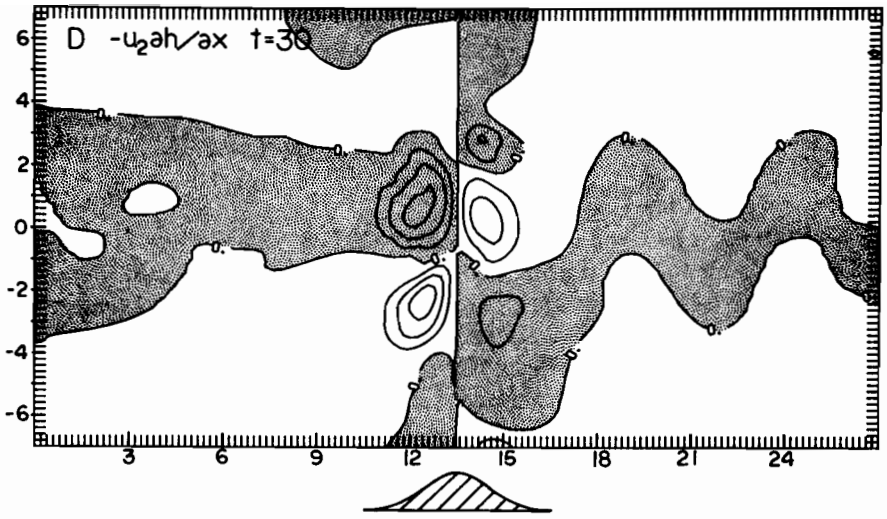

Figure 7. $(-u_2 \partial h/\partial x)$ at t = 30 of case D. Dotted area denotes the negative value.

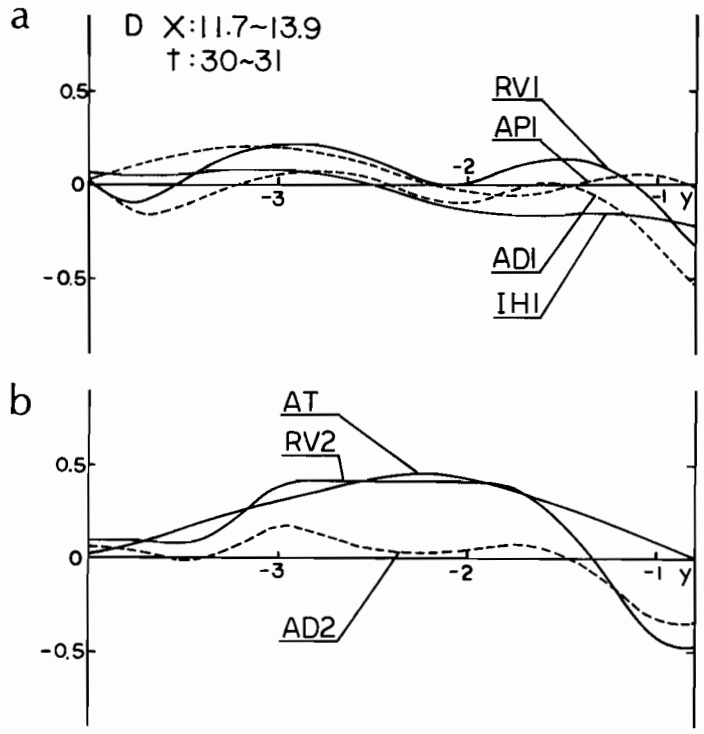

Figure 8. The balance of vorticity integrated from x = 11.7 to x = 13.9 and from t = 30 to t = 31 for case D in (a) the upper layer and (b) the lower layer.

The vorticity balance for E_4 is shown in figure 9, where the region of integration is $13.9 < x < 17.1$, and the time is $30 < t < 31$. The fundamental difference between E_3 and E_4 is that in E_4 the ridge effects take a secondary role. Around $y = 3.2$, the center of E_4, the advection of the relative vorticity in the upper layer is the major source of the variation (decrease) of the relative vorticity. In the region $2 < y < 3$, the neck of M_4, this advection increases the relative vorticity in the upper layer as well as in the lower layer through the variation of the interface height, which results in cutting off the meander, M_4. The ridge effects with a negative value around $y = 3$ take only a role of generating E_4 slightly closer to the jet axis.

Comparing the flow patterns of cases A and B with those of case D, we conjecture analogy of the topographic effects in cases A and B. In terms of the locations relative to the ridge, the eddies and meanders of cases A and B listed in behaviors 3 and 4 of table 4 are similar to the corresponding eddies and meanders of case D. Therefore, we may interpret the mechanisms in cases A and B as in case D; for example, E_2 of case A is strengthened because of the westward flow of the gyres on the western slope.

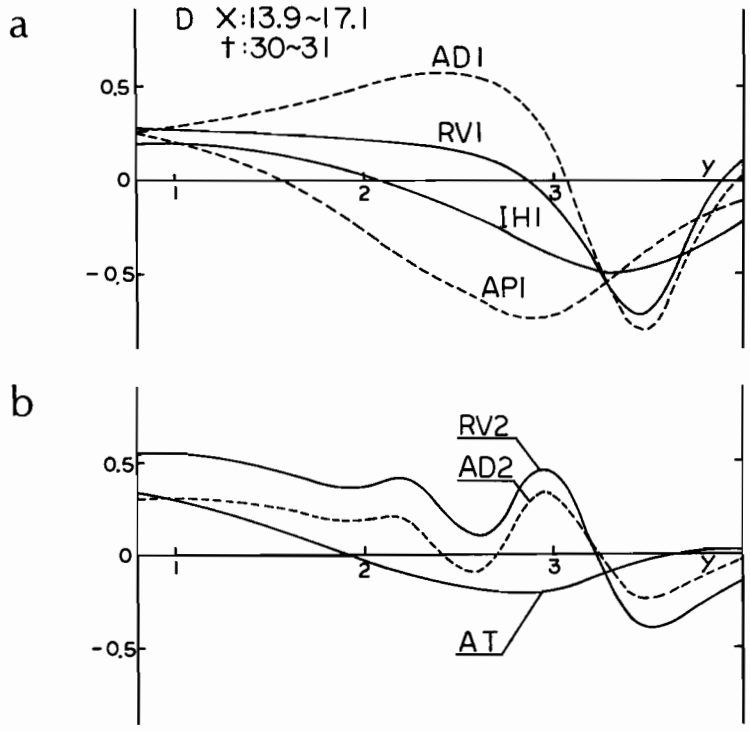

Figure 9. The balance of vorticity integrated from x = 13.9 to x = 17.1 and from t = 30 to t = 31 for case D in (a) the upper layer and (b) the lower layer.

We summarize the analysis in this subsection. The basic concept enables us to interpret the intensification of detached eddies and jet meanders over the ridge as effects of the ridge on the zonal flows associated with the recirculating gyres. The topographic effects denoted by $(-u_2 \partial h/\partial x)$ are sometimes major causes, but there are cases where the topographic effects take a secondary role. Indirect bottom influences, by which the event of detachment propagates downstream faster, cause eddies to be detached more rapidly and closer to the jet axis, even far downstream of the ridge.

5.2 Coalescence of Eddies with the Jet

For the purpose of interpreting behavior 5 in table 4, we look at eddy trajectories and study the effects of the ridge on eddy movement.

In figure 10, we show the trajectories of the detached eddies, E_2, E_3, and E_4, and of the pressure anomalies from which these eddies are detached. The locations of the latter ones are plotted using the anomaly centers in the lower layer, because they are more marked in the lower layer. In the no-ridge case N, the cyclonic detached eddy E_2 travels westward after detachment, and E_4 southeastward. The anticyclonic eddy E_3 travels northwestward. None of these eddies coalesces with the jet, at least until t = 42. The pressure anomalies, L_2, H_3, and L_4, leave from the corresponding eddies toward the other sides of the jet and are located within the recirculating gyres.

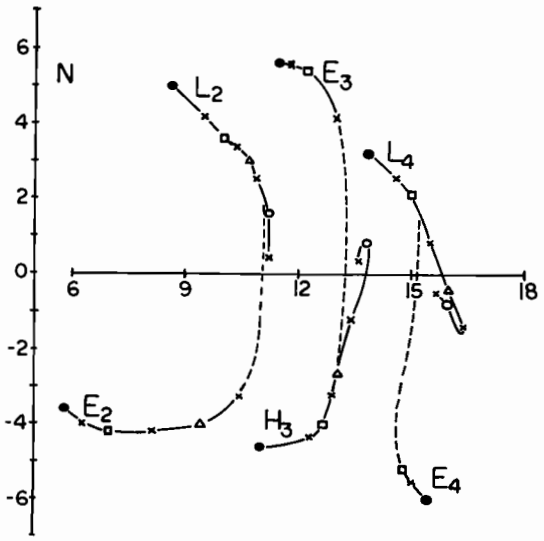

10a.

Figure 10. The trajectories of the detached eddies and of the pressure anomalies from which the eddies are detached. L and H denote the low-and high-pressure anomalies, respectively. The subscript numbers associated with L and H correspond to those of the eddies. No eddy is detached from L_3 of case B. The locations are plotted at t = 21 (x), t = 24 (0), t = 27(x), t = 30 (Δ), t = 33 (x), t = 36 (□), t = 39 (x), and t = 42 (·) for cases (a) N, (B) A, (c) B, (d) C, and (e) D. The side views of the ridge are shown in all figures.

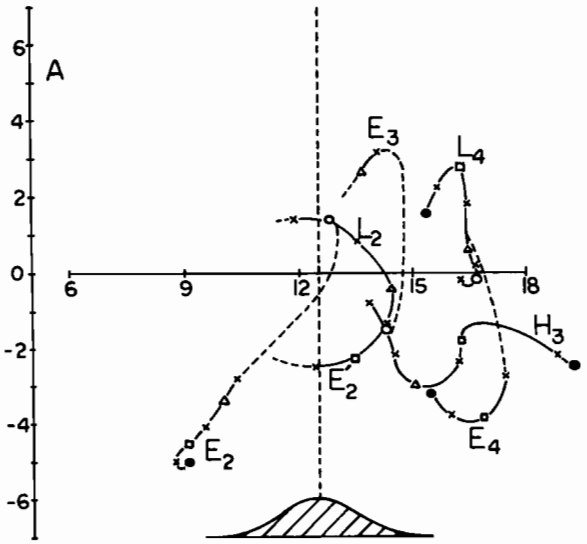

Figure 10b.

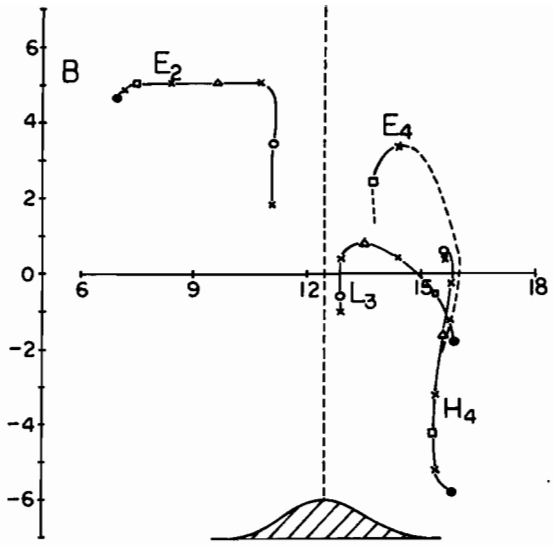

Figure 10c.

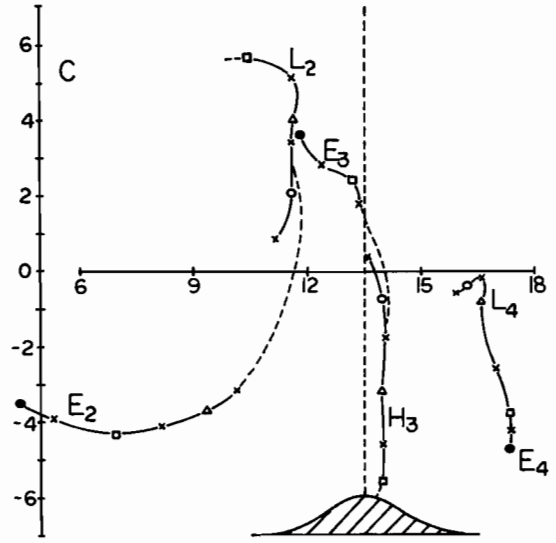

Figure 10d.

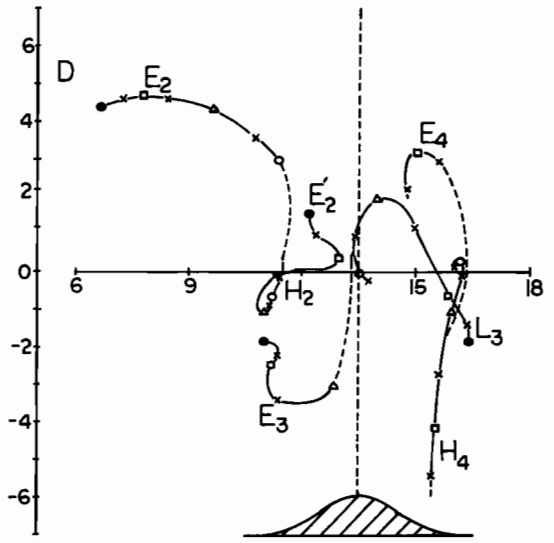

Figure 10e.

Let us look at the four ridge cases. It is clear that E_3 of case A, E_4 of case B, and E_3 and E_4 of case D travel toward and coalesce with the jet. These eddies travel northward on the western slope, or southward on the eastern slope. This movement is consistent with a topographic Rossby wave; that is, eddies move to the left facing the up-slope. The similar tendency is found in the cases of L_2(A), L_3(B), H_3(C), H_2(D), and L_3(D).

In summary, the coalescence of the detached eddies with the jet is interpreted to be a result of a topographic Rossby wave associated with the ridge; eddies and jet would not coalesce without the ridge.

5.3. Jet Splitting

The jet splits into two branches in the region where $9 < x < 14$ at $t = 42$ in case D. The time variations of the flow pattern shown in figure 2 indicate that the cyclonic detached eddy, E_3, travels northward and coalesces with the jet between $t = 36$ and $t = 42$. Then, one branch splits from the major jet and flows around E_3. This south branch tends to expand westward and eastward; that is, it does not keep a strict path around E_3, but tends to flow zonally where $6 < x < 17$. We call this flow pattern jet splitting. Although one condition of the jet splitting is the coalescence of E_3 with the jet, the zonal expansion of the south branch is also necessary for the splitting.

It has been described in subsection 5.2 that the eddy coalesces with the jet because of the ridge. Let us examine whether the ridge is a cause of the zonal extension of the south branch using the method of energy transfers among Fourier components proposed in 4.2.

We look for a correspondence between the flow patterns and zonal wavenumber. The south branch of the splitting jet at $t = 42$ has length of 10, which corresponds to a wavenumber of 0.3 ($= 2\pi/(2 \times 10)$). The original flow pattern at $t = 36$, from which the jet changes to the splitting pattern, is composed of E_3, E_4, M_2, and M_3 in the vicinity of the ridge and has a wavelength of 8; that is, a wavenumber of 0.8 ($= 2\pi/8$).

In figure 11, energy transfers to the flow-components at $t = 36$ are plotted versus zonal wavenumber k, being divided into the transfer caused by the ridge effects, ET, and the transfer not caused by the ridge effects, EA. ET is positive around $k = 0.3$, but negative around $k = 0.8$; that is, the south branch of the jet takes energy, while the eddies at $t = 36$ give energy. It is concluded that the ridge causes the south branch to expand zonally.

The sharp peak of EA around $k = 1.0$ corresponds to meander growth in the eastern part, and the large magnitude for $k < 0.2$ indicates that the interface is going up on the south side and down on the north side of the jet in a large region. Fourier components decomposed in a large region tend to cover characteristics of a local phenomenon. Therefore, ET shows the strong bottom effects on jet splitting, a local phenomenon, although the magnitude of ET is smaller than that of EA.

5.4. Smaller, Divided Gyres

As shown by behavior 7 in table 4, the recirculating gyres are divided into the western and eastern sides of the ridge, and are smaller than those in the no-ridge case N. We compare the gyres of case D indicated by the lower-layer stream function in figure 4 with those of case N in figure 12, because the gyres are stronger in the lower layer than in the upper layer. The gyres at t = 36 in case D are restricted to the region west of the ridge, and are smaller than those at t = 36 in case N. Furthermore, the gyres become smaller from t = 30 to t = 36 in case D, and seem to be divided by the ridge.

In figure 13, the smaller, divided gyres are indicated also by the kinetic energy in the lower layer, $K_2(k)$, associated with the Fourier components at t = 36. The distributions of K_2 show that K_2 is smaller for $k < 0.3$ and larger for $0.4 < k < 0.7$ in the ridge cases, compared with case N. The gyres of case N have length of 11, which corresponds to $k = 0.3$ ($= 2\pi/(2 \times 11)$). At this wavenumber, K_2 of case N is larger than K_2 of all ridge cases. The gyres at t = 36 of case D have length of 8, corresponding to $k = 0.4$ ($= 2\pi/(2 \times 8)$), at which K_2 of all ridge cases is larger than K_2 of case N.

Let us examine the ridge effects on the division of the gyres, using ET, the energy transfers to the Fourier components resulting from topographic effects. ET at t = 30 is shown in figure 14 for the ridge cases. All distributions have peaks around k = 0.6, and are negative for $k < 0.3$. These indicate that both the gyres with k = 0.4 and eddies whose scales are smaller than the gyres take energy from larger-scale flows which are represented by the components with $k < 0.3$.

6. Parameter Study with the Variation of Ridge Shape

In section 3 to 5, only one ridge shape is assumed; $h_o = 1$ and $\ell = 1$. In this section, influences of the ridge on flow patterns are examined for the two cases shown in table 2 with the variations of the height, a maximum of which is denoted by h_o, and the width, a half of which is denoted by $2^{\frac{1}{2}}\ell$. The initial condition and the ridge location are the same as case D in which the ridge influences appear typically compared with cases A, B, and C.

6.1 Halved height ($h_o = 0.5$)

A difference between cases D and DH is that the ridge height is halved in case DH. The flow pattern at t = 42 of case DH is shown in figure 15(a). Major differences in flow patterns are noted in the following: in case DH, E_3 is weaker, E_4 is not absorbed into the jet but parts from the jet, and E_2' which forms on the western slope in case D does not appear. Although E_3 does not coalesce with the jet by t = 42, E_3 seems to coalesce shortly, because that is travelling northward on the western slope similarly to case D.

From the differences mentioned above, it is clear that the ridge influences are much weaker in case DH. However, the coalescence between the

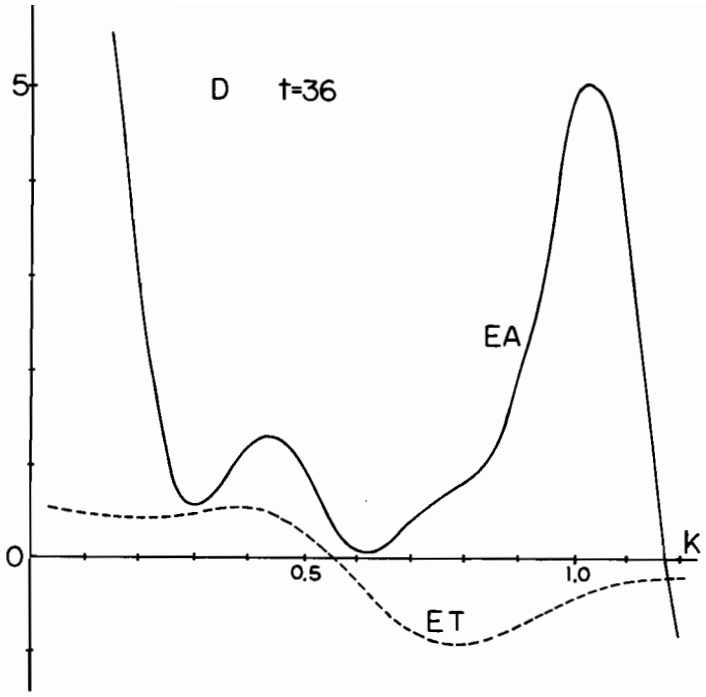

Figure 11. The energy transfers to the Fourier components with zonal wavenumber k, caused by the ridge effects (ET) and not caused by the ridge effects (EA). At t = 36 of case D.

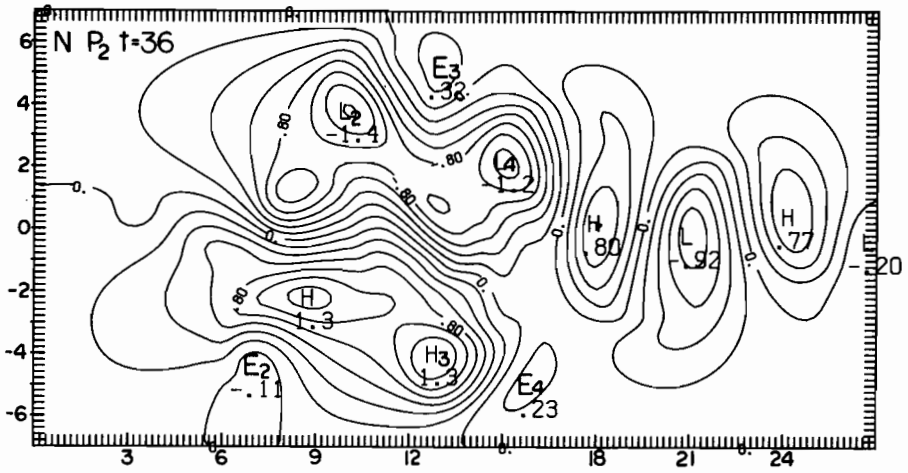

Figure 12. The lower-layer stream function at t = 36 of case N.

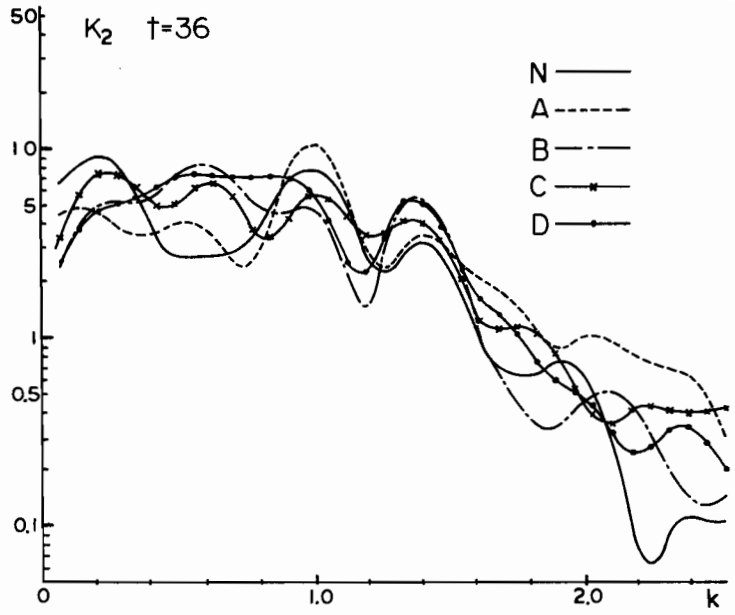

Figure 13. K_2, the kinetic energy in the lower layer associated with the Fourier components versus zonal wavenumber k at t = 36.

$$K_2 = 2\pi \cdot \frac{1-d}{2} \int_{-Y_o}^{Y_o} (|\partial^2 \tilde{p}_2/\partial y^2| + k^2|\tilde{p}_2|)\, dy.$$

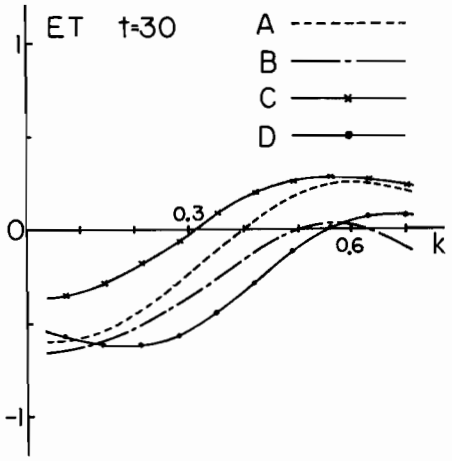

Figure 14. ET, the energy transfers to the k components caused by the bottom topographic effects at t = 30.

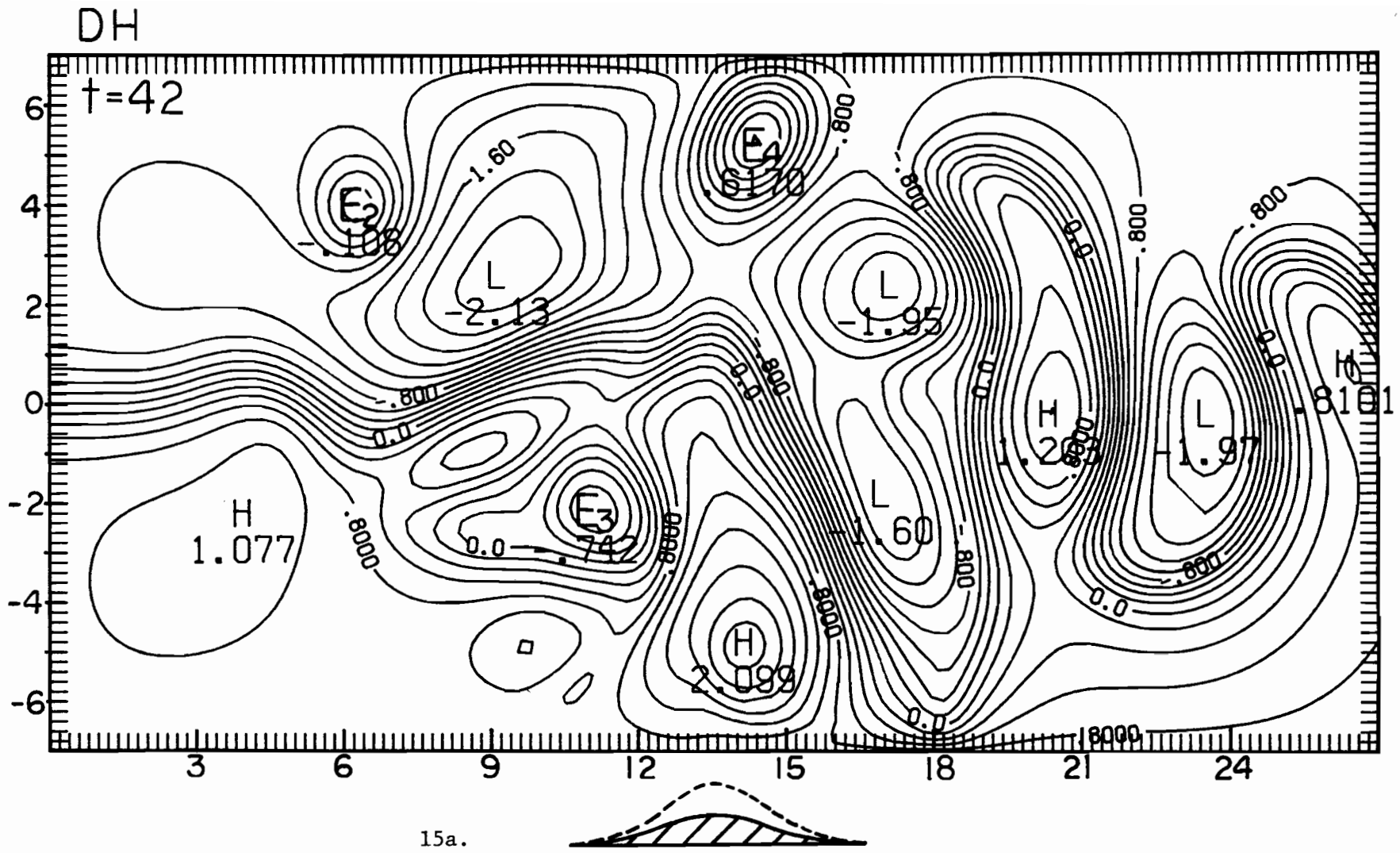

15a.

Figure 15. The upper-layer stream function at t = 42, for cases (a) DH (halved height) and (b) DW (halved width), which are listed in table 2. All flow patterns are compared with that of case D shown in figure 1 (e). The bottom topography is shown by the side view of the ridge in each figure, and the summits are indicated by broken lines.

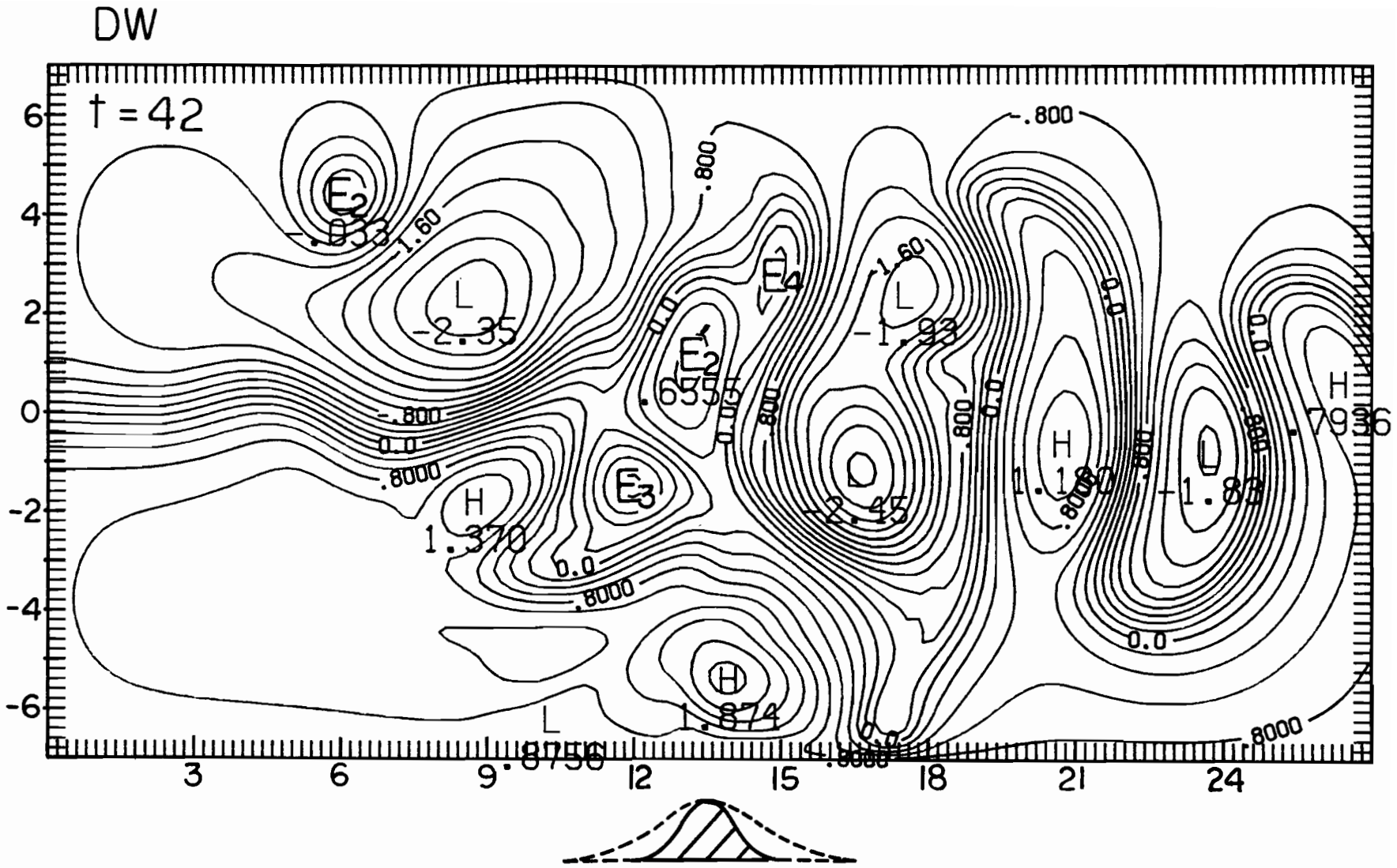
DW
t = 42
E2
E1
E3
E4
L
H
-2.35
1.370
-1.93
-2.45
1.874
1.796
-.800
0.0
.8000
1.60
.6355
-.8756
3
6
9
12
15
18
21
24
6
4
2
0
-2
-4
-6

Figure 15b.

jet and the eddy is observed also in case DH, while that does not occur in the no-ridge case.

6.2 Halved Width (ℓ = 0.5)

A difference between cases D and DW is that the ridge width is halved in case DW. Both flow patterns are similar in the following points: the jet splits into two branches and includes E_3 which is travelling northward on the western slope after southward detachment and E_2' which is generated because of the interaction between the western slope and the eastward flow of the recirculating gyres. Although E_4 is not absorbed into the jet yet by t = 42 of case DW, that will coalesce with the jet shortly, similarly to case D.

The differences in flow patterns between both cases are that E_3 and E_2' have weaker anomalies in case DW, and that splitting branches extend neither westward nor eastward. From the comparisons mentioned above, it is clear that the ridge influences are less significant in case DW. It may be suggested that, on the condition of the same height, stronger ridge effects appear in the case of the half width of 1.4 than 0.7, where an eddy diameter is approximately 2.

7. Comparison with Observations

In the present paper, we have studied the influences of the ridge on the jet. Even if there is no ridge, the jet is unstable enough to have large-amplitude meanders and generate eddies. The ridge strongly affects the process by which eddies are detached from the large-amplitude meanders, and by which the eddies are strengthened and coalesce with the jet. The jet makes many time-variable perturbations which are influenced by the ridge. Among the behaviors shown in table 4, three behaviors are qualitatively compared with flow patterns observed in real oceanic jets over submarine ridges.

As proposed in behavior 3 of table 4, the detached, cyclonic eddies are strengthened south of the jet over the western slope of the ridge, and the anticyclonic eddies north of the jet over the eastern slope. These eddies travel toward the jet and coalesce with the jet, which results in the jet splitting into two branches shown in behavior 6 of table 4. These branches surround the cyclonic eddy mentioned above.

Richardson (1981) showed the observed flow patterns of the Gulf Stream around the New England Seamount Chain. A cyclonic eddy (ring-meander) was located south of the Gulf Stream axis and west of the Chain. Another anticyclonic meander was north of the axis east of the Chain. The Gulf Stream seemed to surround the cyclonic eddy mentioned above.

Similar flow patterns are observed in the Kuroshio. Monthly maps of temperature at 300-m depth made by Bernstein and White (1981) show that strong cyclonic eddies were generated south of the Kuroshio over the western slope of the Shatsky Rise, and that marked anticyclonic eddies appeared north over the eastern slope. The Kuroshio split into two branches surround-

ing the cyclonic eddy. Emery et al. (1980) also showed the splitting immediately west of the Shatsky Rise.

Although the process has not been observed, the numerical solutions are successful in duplicating the flow patterns frequently observed in the Gulf Stream around the New England Seamount Chain as well as the Kuroshio around the Shatsky Rise.

The basic condition for the eddy intensification is that the recirculating gyres are generated north and south of the jet. Richardson (1980) showed that the Gulf Stream is accompanied by a significant recirculating gyre at least on the southern side. In the case of the Kuroshio, there is no observation that confirms the gyres. However, Bernstein and White (1981) suggest a westward, deep mean flow, judging from the fact that time-variable mesoscale disturbances propagate westward in the north and south of the Kuroshio. Therefore, we may conclude that the basic condition is fulfilled.

Behavior 7 in table 3 shows that the recirculating gyres are divided into the western and eastern parts by the ridge, after meanders propagate downstream of the ridge. Richardson (1980) suggested that the New England Seamount Chain and Newfoundland Ridge break the recirculation south of the Gulf Stream into three gyres, using the mean temperature field at a depth of 450 m.

Based on a total fluid-depth of 4 km, a half jet-width of 60 km and a Rossby number of 0.17, the experiments A through D have the ridge with the height of 680 m and the half width of 88 km. The model ridge is much lower than both the New England Seamount Chain and the Shatsky Rise. Even in the case when the height is halved as 340 m, it is observed that a detached cyclonic eddy travels northward on the western slope and coalesces with the jet. Although the two layer model is more sensitive to a bottom topography than is a continuously stratified ocean, the numerical solutions suggest that the Seamount Chain and the Rise are high enough to influence flow patterns in upper oceans.

The half width of 88 km is similar to that of the Shatsky Rise. Although it is difficult to estimate the effective width of the New England Seamount Chain, the half width may be 20 or 30 km. In the case when the width is halved, although the ridge influences are weaker, the ridge has qualitatively the same influences on the eddies whose diameters are three times as large as the half width. This result suggests that the Seamount Chain is wide enough to influence mesoscale eddies.

In terms of the comparison between the model solutions and the observed patterns, the most inadequate point is that no observation has caught the moment of generation. There remain interesting questions to be revealed by further observation: whether the patterns around the ridge are semi-permanent or not permanent but frequent, where the eddies come from, and where they go, together with the variation of eddy strength.

ACKNOWLEDGEMENTS

The author thanks J. Apel for fruitful discussion, H. Mofjeld as PMEL in-house reviewer for improving expressions, P. Richardson of Woods Hole Oceanographic Institution for sharing his manuscript on the new results around the New England Seamount Chain before publication, R. Bernstein and W. White of Scripps Institution of Oceanography for discussion on comparison between theory and observations and for access to their manuscript before publication, and H. Ishii of Maritime Safety Agency of Japan for drifting buoy data. He also thanks J. Chatfield for an editorial review and J. Anderson for making photographs. The work reported here was carried out with the much-appreciated support of 9WGN4010/Pacific Marine Environmental Laboratory where the author worked as a Research Associate of the National Research Council.

REFERENCES

Bernstein, R.L. and W.B. White, 1981: Stationary and traveling mesoscale perturbations in the Kuroshio extension current. J. Phys. Oceanogr., 11, 692-704.

Emery, W.J., C.C. Ebbesmeyer, and J.P. Dugan, 1980: The fraction of vertical isotherm deflections associated with eddies: an estimate from multiship XBT surveys. J. Phys Oceanogr., 10, 885-899.

Gordon, A.L., D.T. Georgi, and H.W. Taylor, 1977: Antarctic polar front zone in the Western Scotia Sea--summer 1975. J. Phys. Oceanogr., 7, 309-328.

Hansen, D.V., 1970: Gulf Stream meanders between Cape Hatteras and the Grand Banks. Deep Sea Res., 17, 495-511.

Huppert, H.E. and K. Bryan, 1976: Topographically generated eddies. Deep Sea Res., 23, 655-679.

Ikeda, M., 1981: Meanders and detached eddies of a strong eastward-flowing jet using a two-layer quasi-geostrophic model. J. Phys. Oceanogr., 11, 526-540.

Ikeda, M. and J.R. Apel, 1981: Mesoscale eddies detached from spatially growing meanders in an eastward-flowing oceanic jet using a two-layer quasi-geostrophic model. J. Phys. Oceanogr., in press.

Ishii, H., 1982: The application of drifting buoys on ocean research. Report of Hydrographic Researches, 17, (March, 1982), in press.

Richardson, P.L., 1980: Gulf Stream system; The average temperature field at a depth of 450 m. International Council for the Exploration of the Sea.

Richardson, P.L., 1981: Gulf Stream trajectories measured with free-drifting buoys. J. Phys. Oceanogr., 11, 999-1010.

Robinson, A.R., J.R. Luyten and F.C. Fuglister, 1974: Transient Gulf Strean meandering. Part 1: An observational experiment. J. Phys. Oceanogr., 4, 237-255.

Roden, G.I., 1977: On long-wave disturbances of dynamic height in the North Pacific. J. Phys. Oceanogr., 7, 41-49.